



Probabilistic Seismic Hazard Assessment for the Arabian Peninsula

YOUSUF AL-SHUIBI,¹ I. EL-HUSSAIN,¹ A. DEIF,^{1,2} ABDULRAHMAN AL-KALBANI,¹ and ADEL M. E. MOHAMED^{1,2}

Abstract—A seismic hazard evaluation in terms of 5% damped peak ground acceleration and spectral acceleration was carried out for the Arabian Peninsula using a probabilistic approach. For this purpose, a revised earthquake catalogue extending from 19 AD to 2015 AD was utilized, including all available earthquakes with magnitude greater than 4.0. The seismic hazard assessment was conducted in the framework of the logic-tree approach to take into account epistemic uncertainties associated with input parameters [seismic source model, recurrence parameters, maximum magnitude, and ground-motion prediction equations (GMPEs)]. A novel seismic source model consisting of 57 seismic zones is proposed as an alternative included in the modeled logic tree. The recurrence parameters were computed mainly using the doubly bounded exponential distribution. Horizontal ground motion in terms of geometric mean acceleration was computed for different spectral periods utilizing GMPEs borrowed from tectonic environments comparable to those surrounding the Arabian Peninsula. The 5% damped seismic hazard values at bedrock conditions were calculated for return periods of 475, 975, and 2475 years. Additionally, uniform hazard spectra for important population centers in the Arabian Peninsula are provided. The highest seismic hazard values were observed along the Zagros, the East Anatolian Fault, and the Gulf of Aqaba–Dead Sea Fault. The provided maps could be used to design the Unified Gulf Building Code.

Key words: Arabian Plate, seismic hazard, building code.

1. Introduction

The Arabian Peninsula has experienced rapid urbanization, increasing population, and strong economic growth in recent years. It has attracted many megaprojects (e.g., Multinational NEUM in Saudi Arabia, Egypt, and Jordan, Expo 2020 in Dubai, the Special Economic Zone at Duqm in Oman, and the World Cup 2022 in Qatar). As human activities

increase, larger portions of the population, land, lifelines, and investments in terms of industry and commerce become more vulnerable to natural hazards, including earthquakes. The Lloyd's City Risk Index (2015) suggests that about US \$85 billion of the Arabian Peninsula's economic output might be at risk due to possible earthquake effects over the next decade. The best way to mitigate the serious consequences of such earthquake risk is to evaluate the seismic hazard, to enhance earthquake-resistant designs and constructions.

The Arabian Peninsula occupies the majority of the Arabian Plate, which is bordered by relatively active tectonic margins of convergent, divergent, and transform type (Fig. 1). The active convergent margins are almost entirely contained in the Makran Subduction Zone, where the Arabian Plate subducts northward below Eurasia along the Sea of Oman (Farhoudi and Karig 1977; Beyer and Bommer 2006), and the ongoing collision since the Oligocene–Miocene of the Arabian Plate with the Eurasian Plate along the Zagros–Bitlis Fold Thrust Belt. Divergent boundaries are evident to the west and south along the spreading centers of the Red Sea and the Gulf of Aden. Major transform margins are present at the East Anatolian Fault to the north, the Gulf of Aqaba–Dead Sea Fault Zone to the northwest, and the Owen Fracture Zone, which separates the Arabian from the Indian Plate to the east.

Earthquake activity in the Arabian Peninsula is mostly confined to plate boundaries, where relative motion between the Arabian Plate and its surroundings takes place (Fig. 2). Although the interior of the Arabian Plate is considered in some studies as a stable craton (Fenton et al. 2006; Aldama et al. 2009), lower levels of seismic activity are observed from Palmyra, the Abdel-Aziz Sinjar area, to the Oman Mountains, in addition to some small to

¹ Earthquake Monitoring Center, Sultan Qaboos University, Muscat, Oman. E-mail: geotec_04@yahoo.com

² National Research Institute of Astronomy and Geophysics, Helwan, Cairo, Egypt.

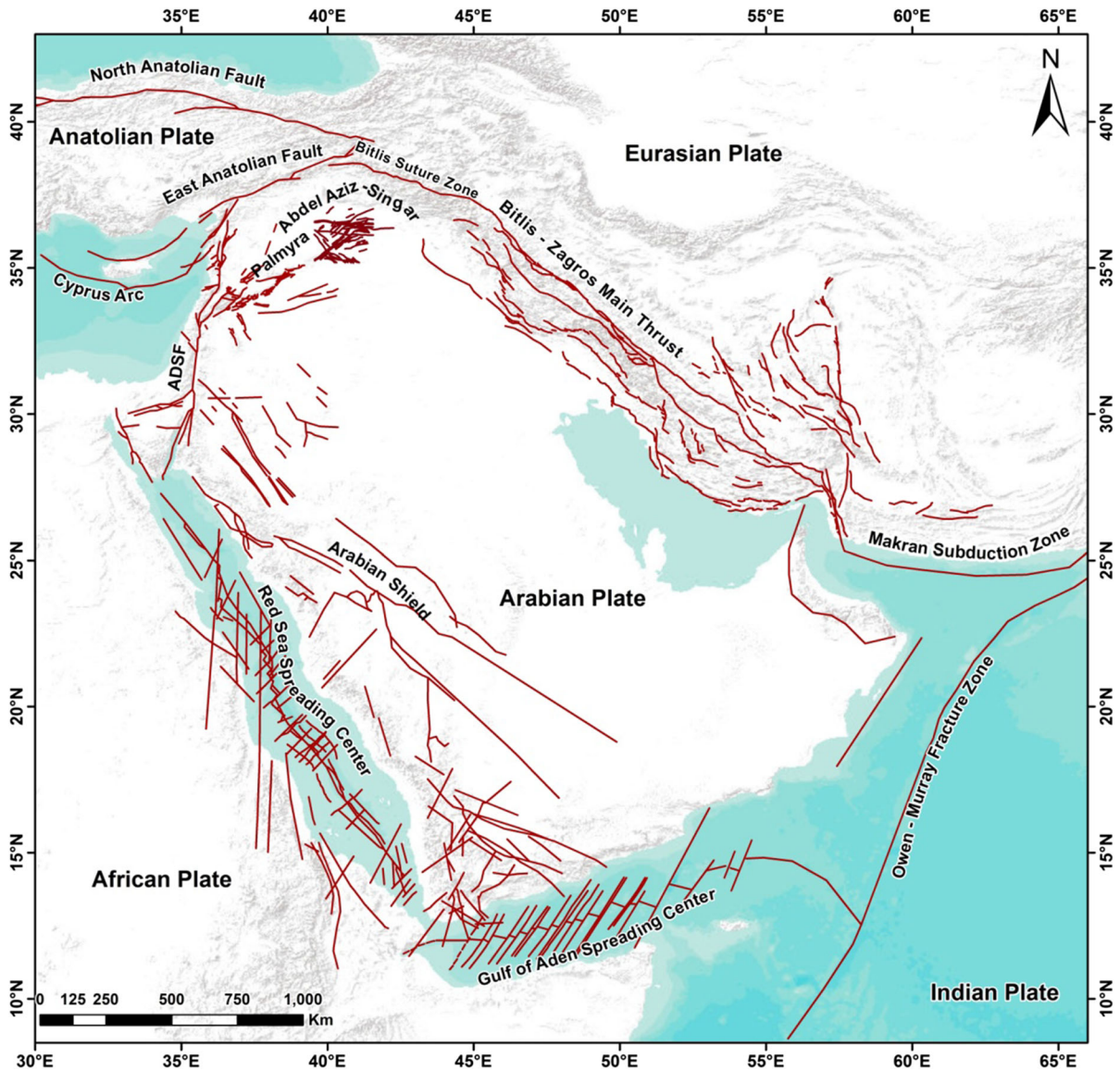


Figure 1

Tectonic elements of the Arabian Plate (Deif et al. 2017). ADSF Gulf of Aqaba–Dead Sea Fault. Brown lines indicate faults

moderate historical and instrumentally recorded earthquakes scattered within the Arabian Peninsula (Deif et al. 2017). With the exception of the Makran Subduction Zone, seismicity in the Arabian Peninsula is dominated by shallow-depth earthquakes at less than 30 km.

To the best of the authors' knowledge, only three seismic hazard studies covering the entire Arabian Peninsula have been conducted. The two early studies

of which the authors are aware were carried out by Al-Haddad et al. (1992, 1994). The main goal of those studies was to provide seismic design criteria for Saudi Arabia, but they extended the hazard values to cover the entire Arabian Peninsula. A single ground-motion prediction equation (GMPE) was used for all the seismic sources regardless of their tectonic nature. They merged the southernmost part of the Zagros Belt with the western part of the Makran

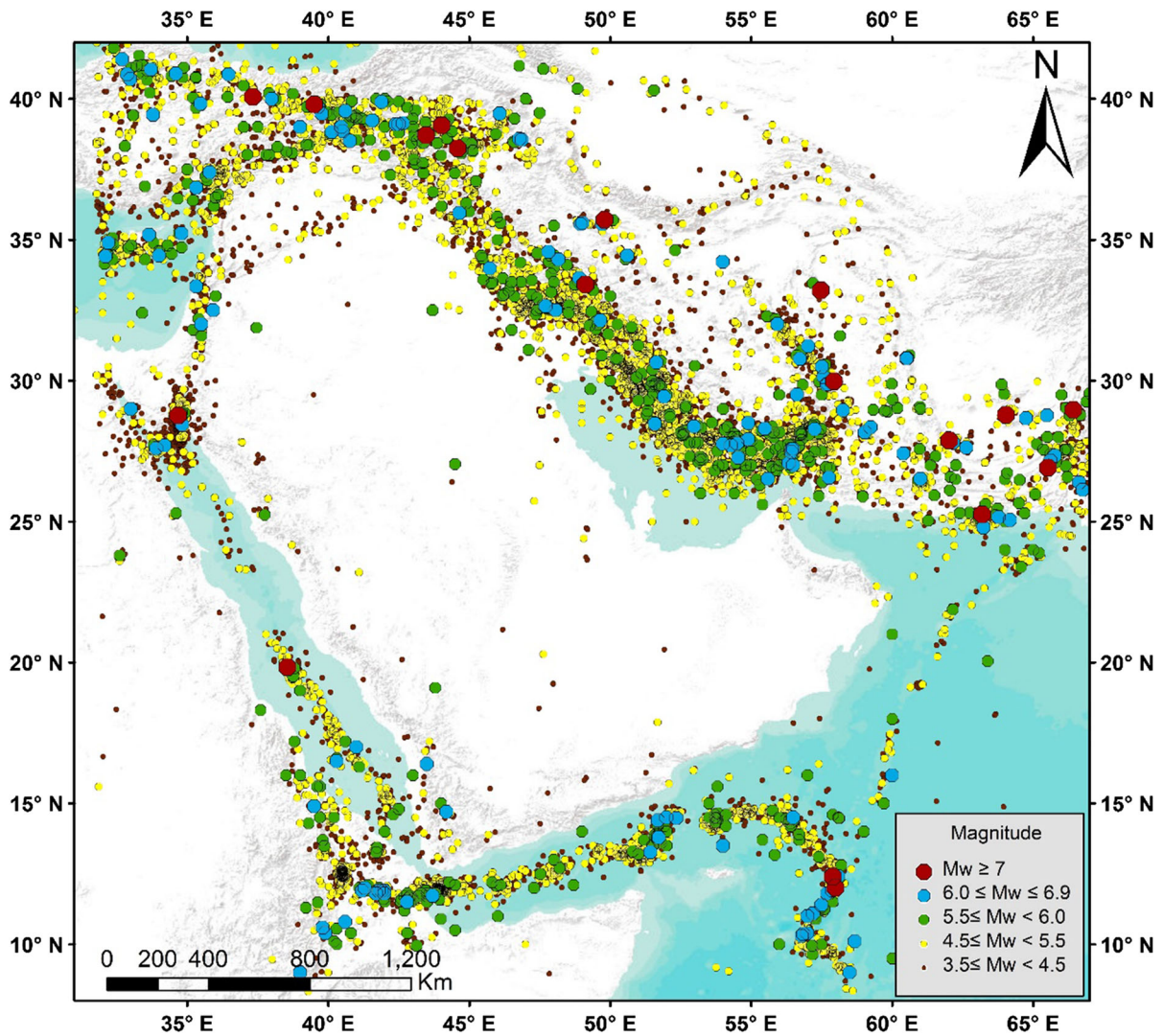


Figure 2
Epicentral distribution of instrumentally recorded earthquakes on the Arabian Plate from 1900 to 2015, (Deif et al. 2017)

Subduction Zone, resulting in high hazard in southwestern Iran. Moreover, no appropriate uncertainty analysis was considered. Finally, they only mapped peak ground acceleration (PGA) values for return periods of 475 and 2475 years. However, PGA is an isolated value on the time record and does not correlate well with the damage potential of shaking.

The third study is a conference paper (not peer reviewed) conducted by Pascucci et al. (2008). Despite being published 5 years after the publication of the active fault map for Iran (Hessami et al. 2003), this important study was not considered in the seismic

source model. Among the many points that are contrary to our opinion regarding the seismic source model, the location of the Aqaba–Dead Sea seismic zone is questionable and should be displaced westward. This study does not provide iso-acceleration maps for the Arabian Peninsula, but rather a table of hazard values for some cities (Dubai, Abu Dhabi, Kuwait, Bahrain, Doha, Jeddah, and Muscat). Many other seismic hazard studies have been published, but only for specific countries in the Arabian Peninsula (e.g., Aldama et al. 2009; El-Hussain et al. 2012; Yilmaz and Yucemen 2015; Babiker et al. 2015;

Onur et al. 2016; Huijjer et al. 2016). The aforementioned studies indicate that most of the Arabian Peninsula could be exposed to low to moderate seismic hazard. However, smaller portions may be exposed to higher hazard levels, which in combination with poor building quality in some countries, could cause serious damage.

Many of the countries in the Arabian Peninsula do not have their own seismic building code. An ongoing project is running to develop a unified building code for the Gulf Cooperation Council (GCC) region. Therefore, the influence of earthquakes on buildings is currently poorly or not considered in many countries in the region. In the light of the above brief discussion, performance of a new seismic hazard study based upon the most recent findings in seismicity, tectonic deformation, active faulting, and slip rate is justified.

A probabilistic seismic hazard assessment (PSHA) was carried out to define the ground-motion parameters for reliable earthquake-resistant design in engineering structures in the Arabian Peninsula. PSHAs are based on the combination of a long-spanning homogeneous earthquake catalogue, seismic source model, recurrence parameters, and appropriate GMPE. The PSHA in the current study was conducted in the framework of a logic tree, allowing inclusion of all earthquake locations, sizes, and path effects, and their epistemic uncertainties. Epistemic uncertainties are considered by selecting proper alternatives for the seismic source model, recurrence parameters, maximum magnitude, and GMPE, yielding various evaluations of expected ground motion. These evaluations were then used to define the mean hazard value and confidence range for each site of interest.

PSHA results are used as the basis for the majority of current seismic building codes worldwide. Regional seismic hazard maps that cover the entire Arabian Peninsula in terms of PGA and 5% damped spectral acceleration (SA) for return periods of 475, 975, and 2475 years are provided herein (corresponding to ground motion likely to be exceeded with 10, 5, and 2% probability in 50 years, respectively).

2. Seismotectonic Setting of the Arabian Plate

The Arabian Plate was formed 25–30 million years ago as a consequence of its detachment from the African Plate due to rifting and opening along the Red Sea and Gulf of Aden axial troughs (Johnson 1998). The seismicity in the Arabian Plate is concentrated along the active tectonics, which are dominated by its subduction under the Eurasian Plate along the Makran Subduction Zone, collision with the Eurasian Plate along the Zagros–Bitlis Thrust, strike-slip faulting along the East Anatolian Fault, Gulf of Aqaba–Dead Sea Fault, and Owen Fracture Zone, and seafloor spreading in the Red Sea and Gulf of Aden (Fig. 1).

The Makran is an east–west striking subduction zone where the floor of the Sea of Oman moves northward below the Eurasian Plate at Iran and Pakistan (Fig. 1). The definition of the Makran area as a subduction zone was pioneered by Stoneley (1974). The Makran northward subduction zone crops out beneath the Sea of Oman and the Arabian Sea at latitude of about 24°N, developing a broad north-dipping deformation zone of thrust faults and accompanied folds that trend to the east (Haghipour et al. 1984; Hessami et al. 2003). Aldama (2009) revealed that the Makran Zone dips at an angle of about 6° from 24°N up to latitude 26.5°N, where the dip angle becomes steeper at about 19°.

Although the seismicity of the Makran seismic source is less than in other Benioff zones worldwide, the potential for generation of great earthquakes ($M > 8.0$) cannot be disregarded. The most eminent earthquake in the Makran Zone took place on 28 November 1945 with M_w 8.1. This event was tsunamigenic and associated with low-angle thrust faulting, causing about 300 fatalities (Ambraseys and Melville 1982). The devastating tsunami impacted the coasts of Pakistan, Iran, as well as Oman, instigating substantial damage and casualties along the Pakistani and Iranian coasts (ASC 2003; Paras-Carayannis 2004). Since then, only one large intermediate-depth (70 km) earthquake with M_w 7.8 has occurred, on 16 April 2013 at the Iran–Pakistan border. This earthquake showed a normal faulting mechanism due to the flexure of the Arabian Plate as it subducts beneath Eurasia. The majority of the

earthquake activity takes place in the eastern section of the Makran Zone, while the western part is apparently quiet, suggesting segmentation (Musson 2009).

The Zagros–Bitlis Thrust Fold Belt runs for about 1500 km from Eastern Turkey to the Strait of Hormuz. This seismic zone is undergoing shortening of about 10 mm/year in the southeast and 5 mm/year in the northwest (Allen et al. 2004; Vernant et al. 2004). This collision zone between the Arabian and Eurasian Plates is characterized by fairly high seismicity along a wide area of about 200–300 km, accounting for the seismic hazard to several surrounding countries. Medium to large earthquakes at shallow depth occur frequently in the Zagros Zone, but rarely exceed M_w 7.0 (Deif and El-Hussain 2012). Most earthquakes in this zone are supposed to take place along blind, active faults without coseismic surface rupture (Berberian 1995). The shallow-depth large earthquake that struck the Iraq–Iran border in November 2017 with M_w 7.3 is not an exception, as no surface rupture was observed, supporting the blind-fault assumption of Berberian (1995). Fault plane solutions show dominant high-angle (40–50°) thrust faults with strikes parallel to the fold axis. Some strike–slip earthquakes occur on faults trending NS oblique to the fold belt, accommodating the inner deformation of the active zone (Deif et al. 2017).

The East Anatolian Fault is a sinistral plate boundary, separating the Arabian Plate from the Anatolian Plate. It runs for about 600 km from the Gulf of Aqaba–Dead Sea Fault toward the northeast, until it joins the North Anatolian Fault (Fig. 1). The East Anatolian Fault shows slip rates of up to 10 mm/year, resulting in large earthquakes with magnitude exceeding 7.0 (Bulut et al. 2012). The largest documented events along the East Anatolian Fault occurred in 1114, 1513, and 1893 with M_s 7.4, 7.4, and 7.1, respectively (Ambraseys and Jackson 1998; Grunthal and Wahlstrom 2012). Only one large earthquake with M_s 6.5 has been generated on this fault in the 20th Century, in 1905. In 2003 and 2010, two earthquakes with M_w 6.4 and 6.1, respectively, hit the East Anatolian Fault in eastern Turkey, killing at least 230.

The Gulf of Aqaba–Dead Sea Fault extends for about 1100 km, joining the Red Sea in the south with

the East Anatolian Fault in the north. It is a sinistral plate boundary, accommodating the relative tectonic movement between the Arabian and African Plates. It is one of the rare plate boundaries on Earth with exposure on the continent. The seismicity along this plate boundary is condensed in the deep areas of the Gulf of Aqaba and Dead Sea. Historical and instrumentally recorded earthquakes indicate that many events with magnitude greater than 7.0 have occurred along the entire fault (Deif et al. 2017). Both seismicity and global positioning system (GPS) measurements indicate the potential for large earthquakes on the main segments along this fault. Low to moderate seismic activity occurs in the intraplate regions, mainly in the north (Fig. 2). Although, the seismicity of the Gulf of Aqaba–Dead Sea Fault is characterized by various fault plane solutions, the focal mechanisms of the large earthquakes verify the geological evidence for its sinistral nature (Bartov et al. 1980; Sneh 1996; Salamon et al. 2003; Palano et al. 2013; El-Hussain et al. 2018).

The Red Sea is a baby ocean about 2000 km long, providing a valuable environment to realize the development from continental rifting to oceanic accretion. The Red Sea starts from 13°N to 28°N, bifurcating at its northern end into the two arms of the Gulfs of Suez and Aqaba, both having different structure. While the Gulf of Suez is developed as a result of tensional movement, the Gulf of Aqaba is an active part of a shear system. Geological and geophysical evidence conclusively confirm the formation of juvenile oceanic crust along parts of the axial trough (e.g., Girdler and Underwood 1985; Rasul et al. 2015). The seafloor spreading process and thus the presence of oceanic crust is fairly recognizable up to 20°N. This active oceanic spreading process is instigating the ongoing drift of the Arabian Peninsula at a rate of about 16 mm/year (ArRajehi et al. 2010). Between 20°N and 23°20'N, the axial trough becomes intermittent, indicating a transition zone. A late-stage continental rift zone occurs north of latitude 23°20'N, consisting of a wide trough with no detectable spreading center.

The earthquake activity along the Red Sea is attributed to the relative motion among the African Plate, Gulf of Aden, and Arabian Plate. The earthquakes that have produced damage and casualties in

populated areas of Yemen and Saudi Arabia are credited to the Red Sea. Most of this earthquake activity is correlated with the axial deep trough and is located between the Gulf of Aden and latitude 20°N. The seismicity levels decrease northward till the Sinai triple junction, where the Red Sea faults meet the NW–SE Gulf of Suez and NE–SW Gulf of Aqaba faults (Fig. 2). The seismicity at this junction is relatively high.

The opening and seafloor spreading along the Gulf of Aden are due to the movement of the Arabian Plate away from Somalia. Geophysical studies have proved that the majority of the floor of the Gulf of Aden is covered by oceanic crust (Coleman 1993). Clear offset of about 160 km appears at the Alula–Fartak Trench. The central axis of the Gulf of Aden is the most seismically active area, along which the seafloor spreading process occurs (Fig. 2). The seismically active zone continues westward to the African Rift Zone. Much less seismicity occurs in the northeast area of the Gulf of Aden. The largest observed earthquake at the Gulf of Aden was M_w 6.6 in 2006. Fault plane solutions show dominant normal as well as strike–slip faulting, confirming the activity of the spreading center and the perpendicular transform faults.

The Owen Fracture Zone and the Murray Ridge form an about 1100-km-long right-lateral transform fault that runs along the eastern margin of the Arabian Plate, detaching it from the Indian Plate. In many studies, these two seismic zones are referred to as the Owen Fracture Zone. This seismic zone has one of the smallest relative motions among major plate boundaries worldwide, with differential motion of about 3 mm/year between the Arabian and Indian Plates (Fournier et al. 2008; DeMets 2008; Akkar and Bommer 2010). With this very low rate of plate motion, the seismicity on these two structures is not expected to be very high. The largest recorded event at the Owen Fracture Zone reached M_w 6.6. Recent earthquakes (as no historical earthquakes are available) on the Murray Ridge were smaller than M_w 6.0. Earthquakes along these plate boundaries are characterized by shallow focal depths. Available focal mechanisms along the Owen Fracture Zone indicate right-lateral strike–slip faulting. Meanwhile, the

Murray Ridge exhibits oblique normal faulting with a right-lateral strike–slip component.

3. Probabilistic Seismic Hazard Assessment

PSHA was first presented by Cornell (1968), and although some amendments have been made to the analysis (e.g., McGuire 1978; Bender and Perkins 1982), the main elements of such hazard assessment remain unaltered. After compiling a reliable earthquake catalogue, PSHA is performed by mixing a seismic source model, earthquake recurrence parameters, and GMPE to create hazard curves.

3.1. Earthquake Catalogue

Earthquake catalogues are a very important outcome of seismological studies as they present a useful dataset for various Earth studies, including seismicity, seismotectonics, and seismic hazard assessment. Earthquake catalogues in combination with the geology and seismotectonic setting of an area of interest are crucial for delineating seismic source models and the recurrence parameters that describe the frequency and severity of earthquakes for each seismic source, which are indispensable for any PSHA.

The earthquake catalogue used in the present study was compiled by Deif et al. (2017). They provided an updated, comprehensive, long, and homogeneous catalogue with a satisfactorily low magnitude threshold for earthquakes located in the Arabian Peninsula and its surroundings. The catalogue was compiled from both historical and instrumentally recorded events, including all earthquake sources with significant hazard on the Arabian Peninsula from 19 AD to 2015 AD. They used a persuasive priority scheme for different data sources, comprising special studies, and local, regional, and international databases. Earthquakes with magnitude down to 4.0 on any magnitude scale were considered as initial entries, since events with lower size are not expected to produce significant risk. Earthquake sizes were originally given on various scales. Therefore, Deif et al. (2017) converted all the reported magnitude scales to M_w using existing relationships and

developed new ones for regions with no reliable conversion equations. Moreover, they developed a special catalogue for the available focal mechanisms in the Arabian Plate.

A typical PSHA relies on the hypothesis that earthquake occurrence follows a Poisson distribution (independent of time and space). The initial catalogue of Deif et al. (2017) lacks homogeneity and completeness in terms of time and space. Therefore, they further processed their earthquake catalogue to check clustering and completeness. All non-Poissonian events were identified and removed by applying three commonly used algorithms, namely those of Gardner and Knopoff (1974), Uhrhammer (1986), and Burkhard and Grunthal (2009). For these three algorithms, earthquakes situated within specific time and space windows are defined based upon the size of the main shock and are considered dependent events and eliminated from the catalogue. Uhrhammer's (1986) algorithm is found to be the most conservative, as it identifies fewer dependent events, leading to higher seismicity rates. Thus, the declustered catalogue resulting from application of the Uhrhammer (1986) algorithm was used in the current study for the PSHA in the Arabian Peninsula. Additionally, Deif et al. (2017) used a simple method provided by Burkhard and Grunthal (2009) to evaluate the temporal magnitude completeness, resulting in subcatalogues with different time and magnitude levels of completeness (for more details, refer to Deif et al. 2017).

3.2. Seismic Source Model

Following the compilation of the earthquake catalogue, the investigated area should be subdivided into a number of seismic source zones. The delineation of these zones is an important component of any seismic hazard assessment. There is no standard procedure for such delineation, and data given by earthquake catalogues alone are insufficient. Therefore, additional information related to the earthquake occurrence process is essential (e.g., geologic information, active faults, recent crustal movement, geophysical investigations, and geodetic data).

For the purpose of seismic hazard assessment, it is preferable to define each particular active fault that

can produce earthquakes with any potential effect on the area of study. This is practically unfeasible for the Arabian Plate because: (1) the Zagros Fold–Thrust Belt is distinguished by the presence of chains of blind thrust faults with no surface displacement and thus the triggering faults have inaccurate locations and slip rates (Berberian 1995); (2) while maps of active faults have been issued for Iran, Turkey, and along the Gulf of Aqaba–Dead Sea Fault, information on active faulting is lacking for the rest of the Arabian Peninsula; (3) the locations of many earthquakes are combined with some uncertainties; (4) several fault zones are characterized by considerable width and inclination. Therefore, seismic source zones in the present study are identified as area instead of line sources.

As this PSHA was performed in the framework of a logic-tree algorithm, two seismic source models were applied in the current study to consider the epistemic uncertainty. The first model (Fig. 3) was developed based on the earthquake activity, together with the geologic and tectonic features of the region. The second model (Fig. 4) generally uses larger zones, attempting to capture the main tectonic elements of the Arabian Plate. The first model represents the current authors' point of view, while the second one mainly combines other authors' opinions (e.g., Tavakoli and Ghafori-Ashtiany 1999; Erdik et al. 2008; Bayrak et al. 2009; Deif et al. 2009; Babiker et al. 2015; Zahran et al. 2016).

The first seismic model comprises 57 seismic zones (Table 1), including the background one. The seismic zones were delineated taking into consideration all the seismic sources that might influence the Arabian Peninsula, including the Makran Subduction Zone, Zagros Fold-Thrust Belt, East Anatolian Fault, Gulf of Aqaba–Dead Sea Fault, Red Sea, Gulf of Aden, Owen Fracture Zone, and Murray Ridge, in addition to the seismic sources inside the Arabian Plate (e.g., Oman Mountains, Yemen, Palmyra, and the Abdel-Aziz Sinjar Area). Details about the geology and seismotectonic features of each seismic zone in addition to the reasons for such delineation and the separation between each pair of zones are given in a specific research paper (El-Hussain et al. 2018). The second seismic source model consists of 36 seismic zones, reflecting the regional tectonic

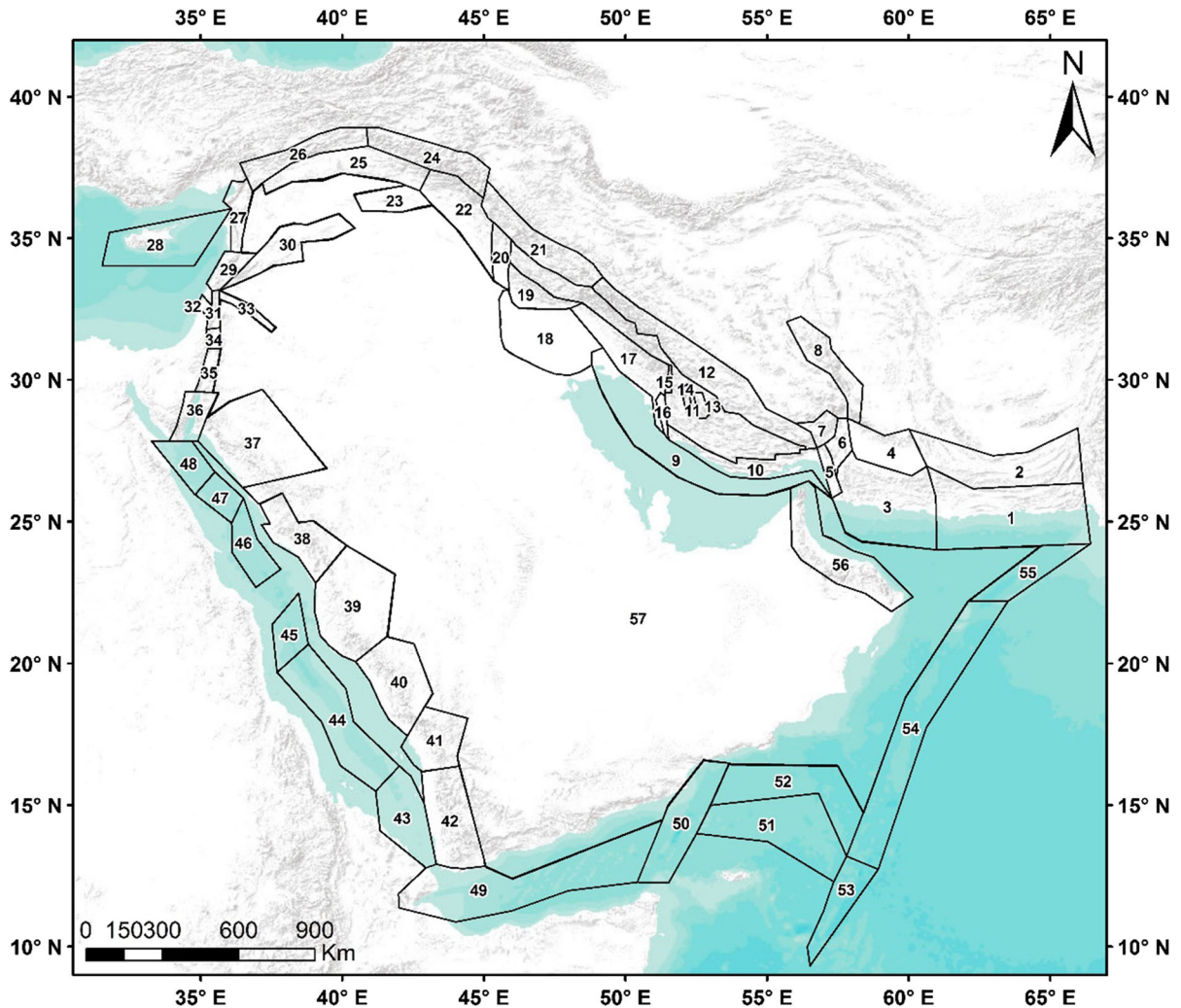


Figure 3
Preferred seismic source model for the Arabian Plate

setting. Weights given for each seismic source model are discussed below in the section on seismic hazard calculation.

3.3. Earthquake Recurrence Coefficients and Maximum Magnitudes

Recurrence relationships represent the distribution of earthquake occurrence with time for various magnitude levels at each seismic source. It is crucial for PSHA, as it is a mean to guesstimate future earthquake activity based upon the rates of past seismic activity. Such a relationship is known to be

first proposed by Gutenberg and Richter (1956). They obtained an exponential recurrence model between the cumulative frequency of earthquakes and the magnitude, and found it appropriate for a broad range of magnitude over large areas. The relationship of Gutenberg and Richter (1956) is open at both the lower and upper end, entailing the impractical assumption that the earthquake size for any area is unlimited and unrelated to the finite dimensions of the seismic sources. Therefore, the earthquake recurrence in the current study was evaluated using a doubly bounded exponential model (Cornell and Vanmarcke 1969) to avoid the drawbacks associated

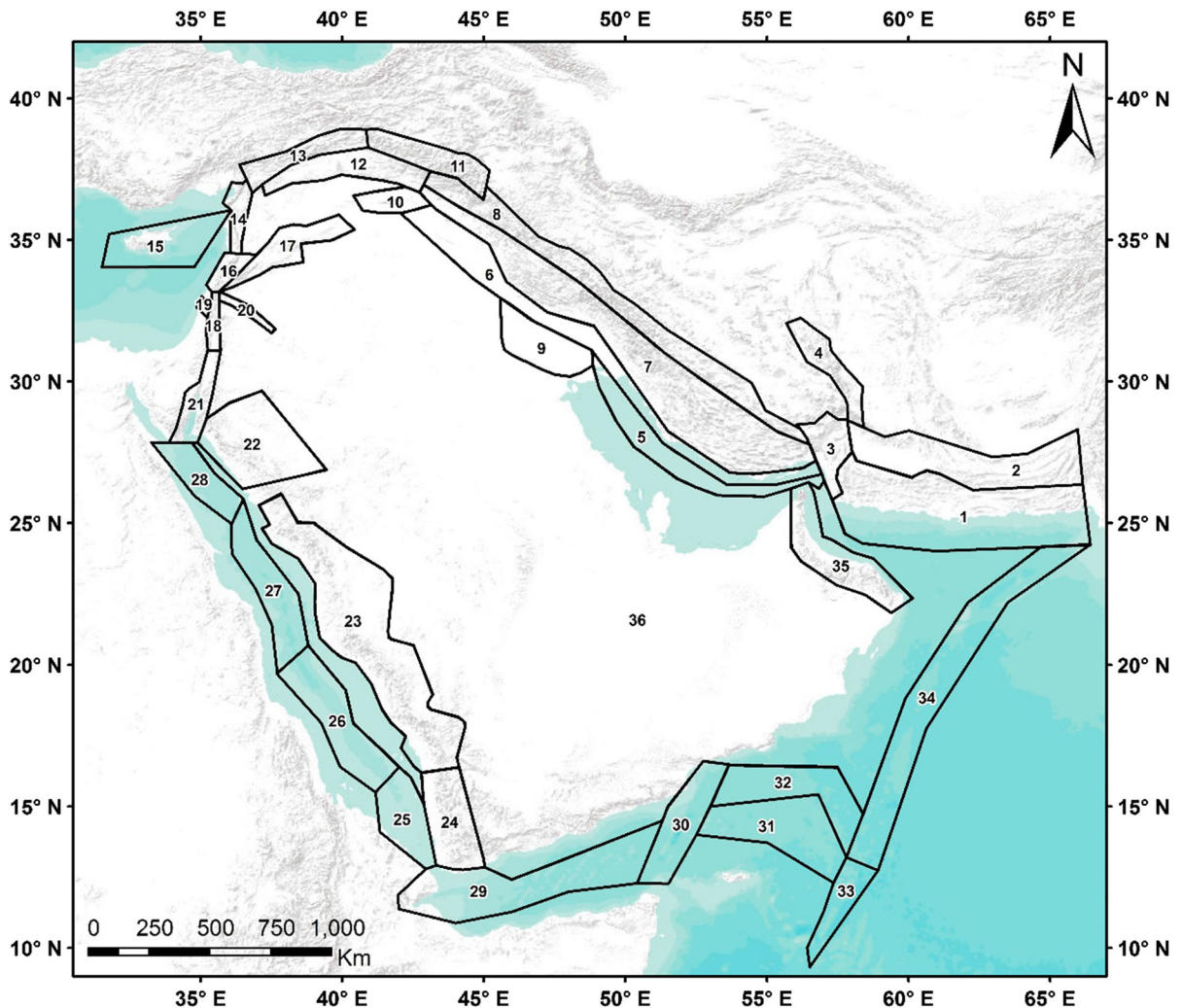


Figure 4
Alternative seismic source model for the Arabian Plate

with the untruncated one of Gutenberg and Richter (1956).

$$N(\geq M) = \alpha \frac{\exp[-\beta(M - M_{\min})] - \exp[-\beta(M_{\max} - M_{\min})]}{1 - \exp[-\beta(M_{\max} - M_{\min})]}, \quad (1)$$

where $\alpha = N(M_{\min})$, M_{\min} is an arbitrary threshold magnitude representing the smallest earthquake that could affect engineered constructions, M_{\max} is the largest magnitude of earthquake that the seismic source is capable to generate, and $\beta = b \times \ln 10$, where b is the slope of the Gutenberg and Richter (1956) model.

Owing to the different completeness levels of the earthquake database (Deif et al. 2017), the coefficient in the Cornell and Vanmarcke (1969) model cannot be determined appropriately using a straightforward regression. Therefore, procedures such as that introduced by Cosentino et al. (1977), Weichert (1980), Dong et al. (1984), and Kijko and Sellevoll (1992), among others, must be applied. The coefficients of the used recurrence relationship for each delineated seismic source, and their standard deviations, were calculated in the present study utilizing the procedure proposed by Kijko and Sellevoll (1992), which makes

Table 1
Recurrence parameters for the preferred source model

Zone no.	Zone name	a	λ	$\sigma\lambda$	b	σb	β	$\sigma\beta$	M_{\max}^{obs}	M_{\max}	σM_{\max}
	All Makran	3.72	6.295	0.832	0.73	0.03	1.67	0.07	8.1	8.4	0.27
Zone 1	Makran East	2.98	1.822	0.371	0.68	0.06	1.57	0.14	8.1	8.4	0.1
Zone 2	Makran Intraplate	2.53	0.860	0.198	0.65	0.06	1.49	0.16	7.3	7.8	0.3
Zone 3	Makran West	2.71	0.680	0.167	0.72	0.08	1.65	0.19	5.9	6.2	0.23
Zone 4	Jaz-Murian	2.35	0.423	0.131	0.68	0.09	1.56	0.2	6.1	6.8	0.82
Zone 5	Zendan Fault	1.95	0.465	0.133	0.57	0.09	1.30	0.2	6.1	6.3	0.22
Zone 6	Jiroft Fault	3.06	1.268	0.271	0.74	0.07	1.70	0.17	5.8	6.0	0.14
Zone 7	Ali Abad	2.97	2.157	0.411	0.66	0.06	1.52	0.14	6.6	6.8	0.18
Zone 8	Gowk Fault	3.12	1.602	0.299	0.73	0.06	1.68	0.13	7.2	7.5	0.34
	All Zagros	4.53	21.625	2.165	0.8	0.02	1.84	0.04	7.4	7.5	0.12
Zone 9	Arabian Gulf	3.30	1.821	0.368	0.76	0.07	1.74	0.16	6.1	6.2	0.26
Zone 10	Zagros Foredeep	3.69	3.359	0.52	0.79	0.05	1.83	0.11	6.7	6.8	0.21
Zone 11	Zagros Simple Fold	4.11	8.820	1.16	0.79	0.03	1.82	0.07	6.8	6.9	0.21
Zone 12	High Zagros	3.53	3.094	0.468	0.76	0.04	1.75	0.1	7.4	7.6	0.24
Zone 13	Sabz-Pushan Fault	2.76	0.686	0.184	0.73	0.08	1.69	0.19	6.1	6.3	0.34
Zone 14	Karebas Fault	2.62	0.314	0.104	0.78	0.09	1.81	0.22	5.4	5.8	0.46
Zone 15	Kazerun Fault	2.97	1.621	0.417	0.69	0.08	1.60	0.19	5.9	6.0	0.21
Zone 16	Borazjan Fault	2.80	0.989	0.281	0.7	0.08	1.61	0.19	5.7	5.8	0.22
Zone 17	Dezful Embayment	3.97	5.340	0.817	0.81	0.04	1.86	0.1	6.7	6.8	0.12
Zone 18	Mesopotamia	3.94	1.670	0.263	0.93	0.08	2.15	0.18	6.4	6.5	0.3
Zone 19	MFF	2.97	1.619	0.31	0.69	0.06	1.59	0.15	6.3	6.4	0.22
Zone 20	Khanaqin Fault	2.92	0.764	0.158	0.76	0.07	1.76	0.16	7.2	7.3	0.32
Zone 21	Posht-e-Kuh Arc	3.60	2.276	0.448	0.81	0.06	1.86	0.14	6.9	7.0	0.31
Zone 22	Kirkuk Embayment	2.93	1.022	0.225	0.73	0.07	1.68	0.17	6.5	6.6	0.3
Zone 23	Abdel-Aziz Sinjar	2.84	0.330	0.108	0.83	0.1	1.91	0.22	5.2	5.4	0.36
Zone 24	Bitlis	3.45	1.355	0.308	0.83	0.09	1.91	0.2	6.8	6.9	0.32
Zone 25	Karacadağ Extension	2.67	0.466	0.122	0.75	0.1	1.72	0.23	6.8	6.9	0.31
Zone 26	East Anatolian Fault	3.97	2.125	0.367	0.91	0.05	2.08	0.12	7.6	7.8	0.34
	All Dead Sea	4.77	4.030	0.7	1.04	0.06	2.40	0.13	7.5	7.8	0.45
Zone 27	Ghab Fault	3.36	1.009	0.222	0.84	0.06	1.94	0.14	7.4	7.5	0.31
Zone 28	Cyprus	4.46	1.982	0.292	1.04	0.05	2.39	0.12	7.0	7.1	0.31
Zone 29	Lebanon Mountains	3.33	0.490	0.132	0.91	0.07	2.11	0.17	7.5	7.8	0.48
Zone 30	Palmyra	3.63	0.423	0.105	1	0.07	2.23	0.17	7.3	7.7	0.52
Zone 31	Jordan Valley	2.79	0.356	0.104	0.81	0.08	1.86	0.19	7.0	7.2	0.38
Zone 32	Carmel Fault	1.59	0.002	0	0.97	0.1	2.23	0.23	6.8	7.0	0.3
Zone 33	Sirhan Fault	2.37	0.031	0	0.97	0.1	2.23	0.23	6.2	6.7	0.3
Zone 34	Dead Sea Basin	3.21	0.216	0.078	0.97	0.08	2.23	0.19	7.3	7.8	0.98
Zone 35	Wadi Araba	3.08	0.210	0.08	0.94	0.09	2.17	0.22	7.0	7.3	0.3
Zone 36	Gulf of Aqaba	4.54	1.648	0.417	1.08	0.08	2.48	0.19	7.3	7.6	0.3
	All Arabian Shield	2.65	0.342	0.123	0.78	0.1	1.80	0.23	5.7	6.5	0.41
Zone 37	Tabuk	2.55	0.118	0.059	0.87	0.1	2.01	0.22	7.4	7.6	0.3
Zone 38	Hejaz	2.13	0.102	0	0.78	0.1	1.80	0.23	5.7	6.2	0.3
Zone 39	Jeddah	1.89	0.059	0	0.78	0.1	1.80	0.23	4.6	5.1	0.3
Zone 40	Tihama	1.78	0.046	0	0.78	0.1	1.80	0.23	4.4	4.9	0.3
Zone 41	Jizan	2.44	0.208	0	0.78	0.1	1.80	0.23	5.2	5.7	0.3
Zone 42	Yemen	3.15	0.518	0.13	0.86	0.08	1.97	0.18	6.3	6.4	0.31
	All Red Sea	3.58	12.550	1.732	0.62	0.03	1.42	0.06	7.8	7.9	0.31
Zone 43	Southern Red Sea	2.96	0.438	0.097	0.83	0.08	1.90	0.18	6.3	6.4	0.32
Zone 44	Central Red Sea	2.95	1.540	0.32	0.69	0.06	1.58	0.14	7.0	7.3	0.34
Zone 45	Transition Red Sea	1.78	0.095	0	0.7	0.1	1.61	0.23	5.2	5.7	0.3
Zone 46	Northern Transition Red Sea	2.27	0.295	0.031	0.72	0.07	1.61	0.12	6.8	6.9	0.31
Zone 47	Northern Red Sea	2.26	0.288	0	0.7	0.1	1.61	0.23	5.5	6.0	0.3
Zone 48	Sinai Triple Junction	3.87	1.165	0.356	0.95	0.09	2.19	0.2	6.6	6.7	0.14
	All Aden	3.53	13.438	2.043	0.6	0.03	1.39	0.07	6.6	6.7	0.12
Zone 49	Western Aden	3.47	6.222	1.059	0.67	0.04	1.55	0.09	6.6	6.7	0.31

Table 1 continued

Zone no.	Zone name	a	λ	$\sigma\lambda$	b	σb	β	$\sigma\beta$	M_{\max}^{obs}	M_{\max}	σM_{\max}
Zone 50	Alula-Fartak	2.34	2.172	0.397	0.5	0.1	1.15	0	6.6	6.7	0.31
Zone 51	Eastern Aden	2.65	4.513	0.793	0.5	0.1	1.15	0	6.1	6.1	0.3
Zone 52	Northeastern Gulf of Aden	1.83	0.357	0.13	0.57	0.09	1.31	0.21	5.8	6.2	0.48
	All Owen	3.32	11.911	1.618	0.56	0.03	1.28	0.07	7.1	7.2	0.12
Zone 53	Southern Owen	2.61	2.127	0.358	0.57	0.05	1.31	0.11	7.1	7.2	0.33
Zone 54	Owen	2.05	0.594	0.16	0.57	0.08	1.31	0.24	6.5	6.8	0.24
Zone 55	Murry Ridge	1.75	0.559	0.193	0.5	0.1	1.15	0	5.9	6.1	0.25
Zone 56	Oman Mountains	2.71	0.243	0.08	0.83	0.09	1.94	0.21	6.0	6.2	0.21
Zone 57	Arabian Background Zone	4.26	2.000	0.342	0.99	0.06	2.29	0.15	6.5	6.6	0.31

Bold font indicates recurrence parameters for regional tectonic units that contain the delineated seismic sources (All Makran, All Zagros, All Gulf of Aqaba–Dead Sea Fault, All Red Sea, All Aden, and All Owen)

Minimum magnitude (M_{\min}) = 4.0 for all zones

allowance for various times of completeness for different magnitude levels.

The recurrence coefficients were calculated for all distinct seismic sources in addition to the regional tectonic units that contain these smaller seismic sources [All Makran (with depth of 27.3 km), All Zagros (with depth of 28.6 km), Zagros strike–slip faults, All East Anatolian Fault (with depth of 20.9 km), All Gulf of Aqaba–Dead Sea Fault (with depth of 11.2 km), All Red Sea (with depth of 17.7 km), All Aden (with depth of 15.3 km), and All Owen (with depth of 17.6 km)]. The recurrence coefficients and their corresponding uncertainties when using the two seismic source models are presented in Tables 1 and 2.

The maximum magnitude was mainly calculated using software provided personally by Prof. Andrzej Kijko, based theoretically on the work of Kijko (2004), Kijko and Singh (2011), and Vermeulen and Kijko (2017). The proposed approach is very flexible, as it combines earthquakes from the incomplete historical epoch with those extracted from complete instrumental data, allowing the entire earthquake catalogue to be apportioned into several time periods with different levels of earthquake completeness. This was done by applying the following equations:

$$M_{\max} = M_{\max}^{\text{obs}} + \int_{M_{\min}}^{M_{\max}} [F_m(m)]^n dm, \quad (2)$$

where $F_m(m)$ is the magnitude cumulative density function (CDF). This expression is valid for any

cumulative density function of magnitude, stating that the maximum expected magnitude for a seismic source (M_{\max}) is equal to the largest already observed magnitude M_{\max}^{obs} in addition to the value of the above integration (Δ).

$$\Delta = \int_{M_{\min}}^{M_{\max}} [F_m(m)]^n dm. \quad (3)$$

As the result of the integral Δ is never negative, M_{\max} will never be less than M_{\max}^{obs} . The integration Δ for the bounded Gutenberg–Richter model is then expressed as

$$\Delta = \int_{M_{\min}}^{M_{\max}} \left[\frac{1 - \exp[-\beta(M - M_{\min})]}{1 - \exp[-\beta(M_{\max} - M_{\min})]} \right]^n dm. \quad (4)$$

Equation (4) indicates that estimation of M_{\max} requires estimation of the following integral:

$$\Delta = \int_{M_{\min}}^{M_{\max}} \left[\frac{1 - \exp[-\beta(M_{\text{obs}} - M_{\min})]}{1 - \exp[-\beta(M_{\max} - M_{\min})]} \right]^n dm. \quad (5)$$

As the integration in Eq. (5) is difficult to estimate analytically, Kijko (2004) replaced $[F_m(m)]^n$ by its Cramer (1961) approximation $\exp\{-n[1 - F_m(m)]\}$ to facilitate solution of the integration, resulting in M_{\max} .

To conduct an appropriate statistical assessment for seismic sources with very few earthquakes, the maximum magnitudes were calculated by adding 0.5 magnitude units to the maximum observed magnitude in the earthquake catalogue. The maximum magnitudes are listed in Tables 1 and 2 for each seismic zone.

Table 2
Recurrence parameters for the alternative source model

Zone no.	Zone name	a	λ	$\sigma\lambda$	b	σb	β	$\sigma\beta$	M_{\max}^{obs}	M_{\max}	σM_{\max}
Zone 1	Southern Makran	3.10	2.20	0.392	0.69	0.05	1.59	0.12	8.1	8.4	0.2
Zone 2	Northern Makran	2.80	1.20	0.237	0.68	0.06	1.57	0.14	7.8	8.1	0.2
Zone 3	Transition Zone	3.38	3.80	0.604	0.7	0.04	1.62	0.1	6.6	6.7	0.22
Zone 4	Gowk Fault	3.12	1.60	0.299	0.73	0.06	1.68	0.13	7.2	7.5	0.34
Zone 5	Arabian Gulf	2.61	0.71	0.175	0.69	0.08	1.59	0.19	5.8	6.0	0.26
Zone 6	Zagros Foredeep	4.20	3.00	0.467	0.93	0.04	2.14	0.1	7.3	7.6	0.35
Zone 7	Zagros Simple Fold	4.27	9.75	0.858	0.82	0.02	1.89	0.05	6.8	6.9	0.21
Zone 8	Zagros Main Thrust	4.12	2.75	0.381	0.92	0.04	2.11	0.09	7.4	7.7	0.4
Zone 9	Mesopotamia	3.09	0.45	0.14	0.86	0.07	1.97	0.21	5.7	6.1	0.41
Zone 10	Abdel Aziz-Sinjar	2.84	0.33	0.108	0.83	0.1	1.91	0.22	5.2	5.4	0.36
Zone 11	Bitlis	3.45	1.36	0.308	0.83	0.09	1.91	0.2	6.8	6.9	0.32
Zone 12	Karacadağ Extension	2.67	0.47	0.122	0.75	0.1	1.72	0.23	6.8	6.9	0.31
Zone 13	East Anatolian fault	3.97	2.13	0.367	0.91	0.05	2.08	0.12	7.6	7.8	0.34
Zone 14	Ghab Fault	3.36	1.01	0.222	0.84	0.06	1.94	0.14	7.4	7.5	0.31
Zone 15	Cyprus	4.46	1.98	0.292	1.04	0.05	2.39	0.12	7.0	7.1	0.31
Zone 16	Lebanon Mountains	3.33	0.49	0.132	0.91	0.07	2.11	0.17	7.5	7.8	0.48
Zone 17	Palmyra	3.63	0.42	0.105	1	0.07	2.23	0.17	7.3	7.7	0.52
Zone 18	Dead Sea	3.21	0.45	0.115	0.89	0.07	2.06	0.16	7.3	7.8	0.58
Zone 19	Carmel Fault	1.59	0.002	0	0.97	0.1	2.23	0.23	6.8	7.0	0.3
Zone 20	Sirhan Fault	2.37	0.031	0	0.97	0.1	2.23	0.23	6.2	6.7	0.3
Zone 21	Aqaba	4.72	1.33	0.29	1.15	0.07	2.64	0.15	7.4	7.7	0.2
Zone 22	Tabuk	2.55	0.12	0.059	0.87	0.1	2.01	0.22	7.4	7.6	0
Zone 23	All Arabian Shield	2.65	0.34	0.123	0.78	0.16	1.79	0.36	5.7	6.5	0.47
Zone 24	Yemen	3.07	0.52	0.165	0.84	0.09	1.94	0.2	6.3	6.9	0.79
Zone 25	Southern Red Sea	2.96	0.44	0.097	0.83	0.08	1.90	0.18	6.3	6.4	0.32
Zone 26	Central Red Sea	2.95	1.54	0.32	0.69	0.06	1.58	0.14	7.0	7.3	0.34
Zone 27	Red Sea Transition Zone	2.44	0.30	0.101	0.74	0.08	1.70	0.19	6.8	7.1	0.32
Zone 28	Northern Red Sea	3.84	1.09	0.309	0.95	0.08	2.19	0.18	6.6	6.8	0.24
Zone 29	Western Aden	3.47	6.22	1.059	0.67	0.04	1.55	0.09	6.6	6.7	0.31
Zone 30	Alula-Fartak	2.34	2.17	0.397	0.5	0	1.15	0	6.6	6.7	0.31
Zone 31	Eastern Aden	2.65	4.51	0.793	0.5	0	1.15	0	6.1	6.1	0.3
Zone 32	Northeastern Gulf of Aden	1.83	0.36	0.13	0.57	0.09	1.31	0.21	5.8	6.2	0.48
Zone 33	Southern Owen	2.61	2.13	0.358	0.57	0.05	1.31	0.11	7.1	7.2	0.33
Zone 34	Owen	2.40	1.00	0.234	0.6	0.07	1.39	0.16	6.5	6.7	0.28
Zone 35	Oman Mountains	2.71	0.24	0.08	0.83	0.09	1.94	0.21	6.0	6.2	0.21
Zone 36	Arabian Background Zone	4.26	2.00	0.342	0.99	0.06	2.29	0.15	6.5	6.6	0.31

Minimum magnitude (M_{\min}) = 4.0 for all zones

3.4. Ground-Motion Prediction Equations (GMPEs)

The role of the ground-motion prediction equation (GMPE) in the PSHA is to predict what ground-motion value will be observed at a site of interest as a function of magnitude and distance from a specified seismic source. They have a significant impact on the results of the seismic hazard. Uncertainties in GMPEs could be significant due to many factors such as doubts regarding earthquake physics, including the earthquake mechanism and rupture process, and due to site response and unknown details of the three-dimensional (3D) crustal structure. Moreover, they

may be the largest contributor to uncertainties in seismic hazard evaluation. The scatter on ground motion in terms of the standard deviation of each GMPE is an important factor and can be utilized to consider the inconsistency of ground motion.

It would be ideal to use a GMPE that is derived using local strong-motion data, but this is unfeasible due to the lack of such data for the Arabian Peninsula. Therefore, it is obligatory to use GMPEs developed for elsewhere in the world. Seven different GMPEs were considered together within a logic-tree framework to consider the decay of the seismic waves with

Table 3
Main features of the utilized ground-motion prediction equations (GMPEs)

GMPE	Mag.	M_{\max}	Dist.	D_{\max}	H. comp.	Faulting mechanism	Tectonic env.	Model 1	Model 2
Youngs et al. (1997)	M_w	8.2	R_{rup}	500	Geometric mean	Interface/in-slab	Subduction	Zones 1, 2, 3, 4, and 28	Zones 1, 2, and 15
Atkinson and Boore (2003)	M_w	8.3	R_{rup}	550	Random horizontal	Interface/in-slab	Subduction	Zones 1, 2, 3, 4, and 28	Zones 1, 2, and 15
Atkinson and Boore (2006)	M_w	8	R_{rup}	1000	Unspecified	Unspecified	Stable regions	Zones 37, 38, 39, 40, 41, and 57	Zones 22, 23, and 36
Zhao et al. (2006)	M_w	8.4	R_{rup}	300	Geometric mean	Reverse—strike slip	Shallow active and subduction	All zones	All zones
Chiou and Youngs (2008)	M_w	8.5	R_{rup}	200	Average horizontal component	Strike slip—reverse and normal	Shallow active crust	All zones except zones 1, 3, and 28	All zones except zones 1 and 15
Akkar and Bommer (2010)	M_w	7.6	R_{JB}	100	Geometric mean	Strike slip—reverse and normal	Shallow active crust	All zones except zones 1, 3, and 28	All zones except zones 1 and 15
Campbell (2003)	M_w	8.2	R_{rup}	1000	Geometric mean	Unspecified	Stable regions	Zone 57	Zone 36

distance for different magnitude levels. Accounting for the epistemic uncertainty in the ground-motion calculation is done in the present study by applying at least three GMPEs appropriate for each tectonic environment. This consequently involves several various assessments of hazard levels, accounting for the epistemic uncertainty associated with not knowing the actual attenuation characteristics in the Arabian Peninsula. All the selected GMPEs have been extensively used in seismic hazard analyses worldwide and are recommended for the Middle East region by Delavaud et al. (2012) and Douglas et al. (2014) based upon their personal judgment and analytical testing of many GMPEs for the Earthquake Model of the Middle East (EMME).

With the exception of the seismic sources of the Makran Subduction Zone, Cyprus, and the Background Seismic Zone, the remaining seismic zones are considered as crustal shallow active sources. We used the models of Akkar and Bommer (2010), Chiou and Youngs (2008), and Zhao et al. (2006) to model the ground motion of earthquakes occurring within the active shallow crustal seismogenic zones. The GMPEs of Youngs et al. (1997), Atkinson and Boore (2003), and Zhao et al. (2006) are used to model the ground motion of the Makran and Cyprus seismic

zones. The definition of the Arabian Peninsula as a stable craton is not unambiguously confirmed (Al-dama et al. 2009). Thus, for earthquakes occurring within the stable Arabian Peninsula (Background Seismic Zone), models borrowed from stable regions (Atkinson and Boore 2006; Campbell 2003) were used in conjunction with GMPEs for active shallow zones (Akkar and Bommer 2010; Chiou and Youngs 2008; Zhao et al. 2006).

A summary of the properties of the suite of selected GMPEs is given in Table 3. Merging more than one GMPE in a logic tree during the PSHA may require making some transformations due to the different definitions existing in both the predicted and explanatory parameters of each ground-motion equation. Thus, the selected alternatives in the context of the logic tree should be converted into joint metrics (Bommer et al. 2005; El-Hussain et al. 2012).

All the GMPEs applied in the current study use the moment magnitude scale to express earthquake size. Therefore, all of them are compatible with the magnitude scale in the earthquake catalogue (Deif et al. 2017) with no need for any transformation.

Using different metrics for the distance from the seismic source to the site of interest could be a source of incompatibility. In contrast to most of the selected

GMPEs that use R_{rup} as a distance metric, Akkar and Bommer (2010) use R_{JB} . Fortunately, the software used to perform the hazard calculations (EZ-FRISK) can use tabulated ground-motion values to define the level of ground motion corresponding to a particular magnitude–distance scenario. This framework enables different distance metrics to be implemented very easily with no need for distance conversion.

The selected GMPEs utilize different classifications for the horizontal component of ground motion, depending on the handling of the two horizontal traces from each record. When GMPEs using various horizontal-component classifications are merged in a logic-tree framework, modifications must be made to both the median values of the predicted ground-motion parameter and for the combined aleatory variability to realize compatibility among the GMPEs. In the present PSHA, the ground motion is identified as the geometric mean of the two horizontal components. GMPEs for which the horizontal ground motion is not defined as the geometric mean of the two horizontal components were adjusted to this definition using the relationships of Beyer and Bommer (2006), who provided ratios of both medians and standard deviations for all existing horizontal-component definitions with respect to the geometric mean. Appropriate fault plane solutions have been specified for each seismic source zone, which allows more specific characterization of seismic sources and ensures compatibility of the selected GMPEs.

3.5. Seismic Hazard Calculation

The PSHA in the current study was carried out for bedrock conditions ($V_{S30} = 760$ m/s) within a logic-tree framework, allowing alternatives for each decision-making process to be combined in the hazard assessments. In the logic-tree algorithm, branching in each calculation step was applied to represent the various alternatives considered (4860 branches are considered in the designed logic tree for the final hazard calculations). The pop-up branches from each node were assigned weightings in such a way that their sum was unity, reflecting the relative confidence in each alternative. The hazard results were then obtained by following each branch on the logic tree; the weightings along all the branches in each

calculation were multiplied to obtain the final weight for the hazard results for a particular branch. The final results were then calculated using a weighted average procedure to obtain the hazard curve for each site of interest.

In the present study, the weights given to each alternative are depicted in Fig. 5. There are five components of the logic tree, related to the seismic source model, recurrence parameters, maximum source magnitude, maximum observed magnitude in the Western Makran seismic zone, and GMPEs. The weightings were assigned to each branch based on subjective discussion among the research team of the current study.

The formal analysis of the uncertainties in the seismic source model included seismic source model 1 (Fig. 3), which reflects the current authors' point of view, as well as seismic source model 2 (Fig. 4), reflecting the regional tectonic setting. However, source model 2 lacks a higher level of resolution, as it is not correlated with known individual active faulting structures with potential to generate earthquakes of considerable hazard, which is necessary when developing a seismic source model for the PSHA. Thus, it is justified to give a weight of 0.8 to the first seismic source model but only 0.2 to the second.

The maximum earthquake in the Western Makran seismic zone is controversial, depending on whether the earthquake in 1483 took place in this seismic zone or not. If this earthquake occurred in the western segment of Makran with M 7.7 (Ambraseys and Melville 1982), the maximum magnitude would be 8.2. However, Ambraseys and Melville (1982) classified the location of this event as very approximate, being large but with insufficient details. On the other hand, if this event was a local earthquake in Hormuz Musson (2009), the maximum magnitude in Western Makran is calculated to be 6.2. The first assumption is given weight of 0.3 as it depends on a rather older study with uncertain earthquake location, while the second assumption is given weight of 0.7.

Regarding the recurrence parameters [β , λ , and maximum magnitude (M_{max})] of each seismic source, the seismic hazard was computed using the mean, adding and subtracting one standard deviation, sequentially. The mean value of each recurrence

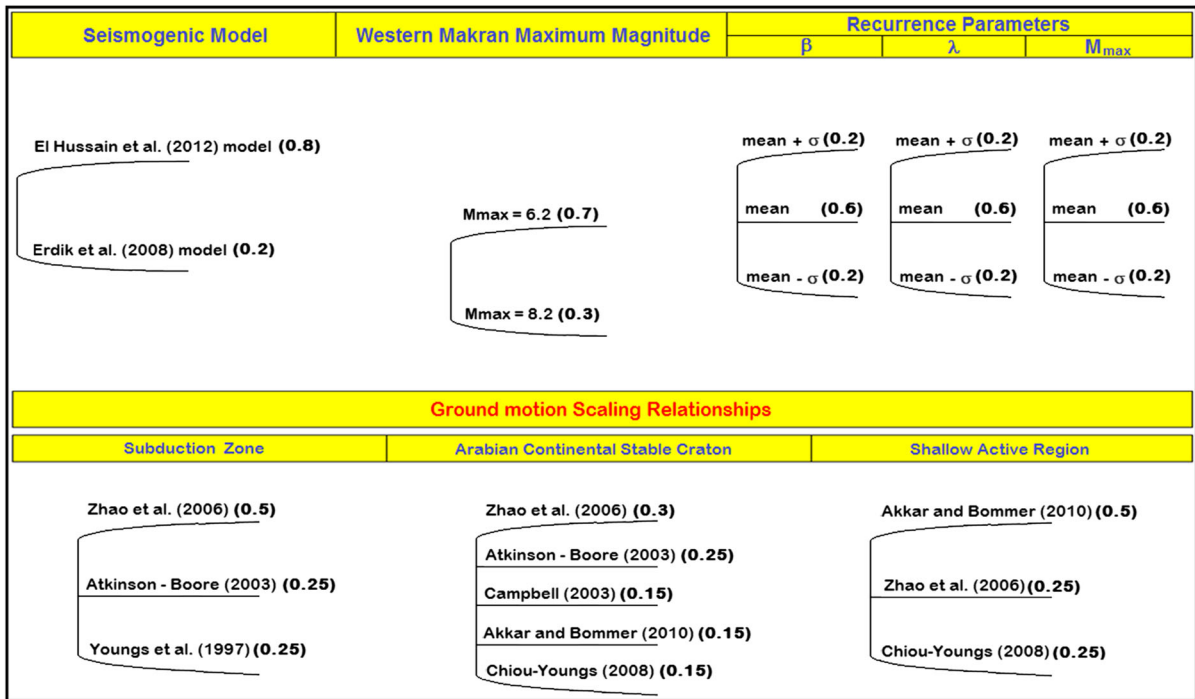


Figure 5

Elements of the logic tree utilized for the current probabilistic seismic hazard assessment for the Arabian Plate; bold numbers are the weights assigned for each alternative

parameter was allocated weight of 0.6, while the recurrence parameters plus and minus one standard deviation were assigned weight of 0.2. The selection of these weights was guided mainly by some relatively recent publications (e.g., Aldama et al. 2009; Sawires et al. 2016).

For the GMPEs in active shallow seismic zones, the Akkar and Bommer (2010) model was assigned weight of 0.5, while each of those of Zhao et al. (2006) and Chiou and Youngs (2008) was assigned equal weight of 0.25. This was decided because the Akkar and Bommer (2010) model is relatively more recent, used some strong-motion records from the Middle East, and was found to be among those appropriate for use in the Middle East (Delavaud et al. 2012). Regarding the GMPEs for the stable Arabian Peninsula, the models of Zhao et al. (2006) and Atkinson and Boore (2003) were privileged with allocated weight of 0.3 and 0.25, respectively, with the remaining weight of 0.45 being divided equally among the other three active shallow models. The GMPEs for shallow active environment were

introduced for this stable area because the nature of the Arabian Plate as a stable craton has no conclusive evidence (Aldama et al. 2009). For the subduction zone GMPEs, the Zhao et al. (2006) model was favored with weight of 0.5, with the remaining weight of 0.5 being divided equally between the models of Atkinson and Boore (2003) and Youngs et al. (1997).

4. Results

Seismic hazards were computed for return periods of 475, 975, and 2475 years within the logic-tree framework over a $0.2^\circ \times 0.2^\circ$ grid, covering the entire Arabian Peninsula and its surroundings. These return periods were selected as they become important references in most seismic design codes. Hazard values were estimated at 9334 computation nodes and utilized to develop maps (using ArcGIS 10.1 software) for the horizontal PGA and 5% damping response spectra for bedrock site conditions with reference to the National Earthquake Hazards

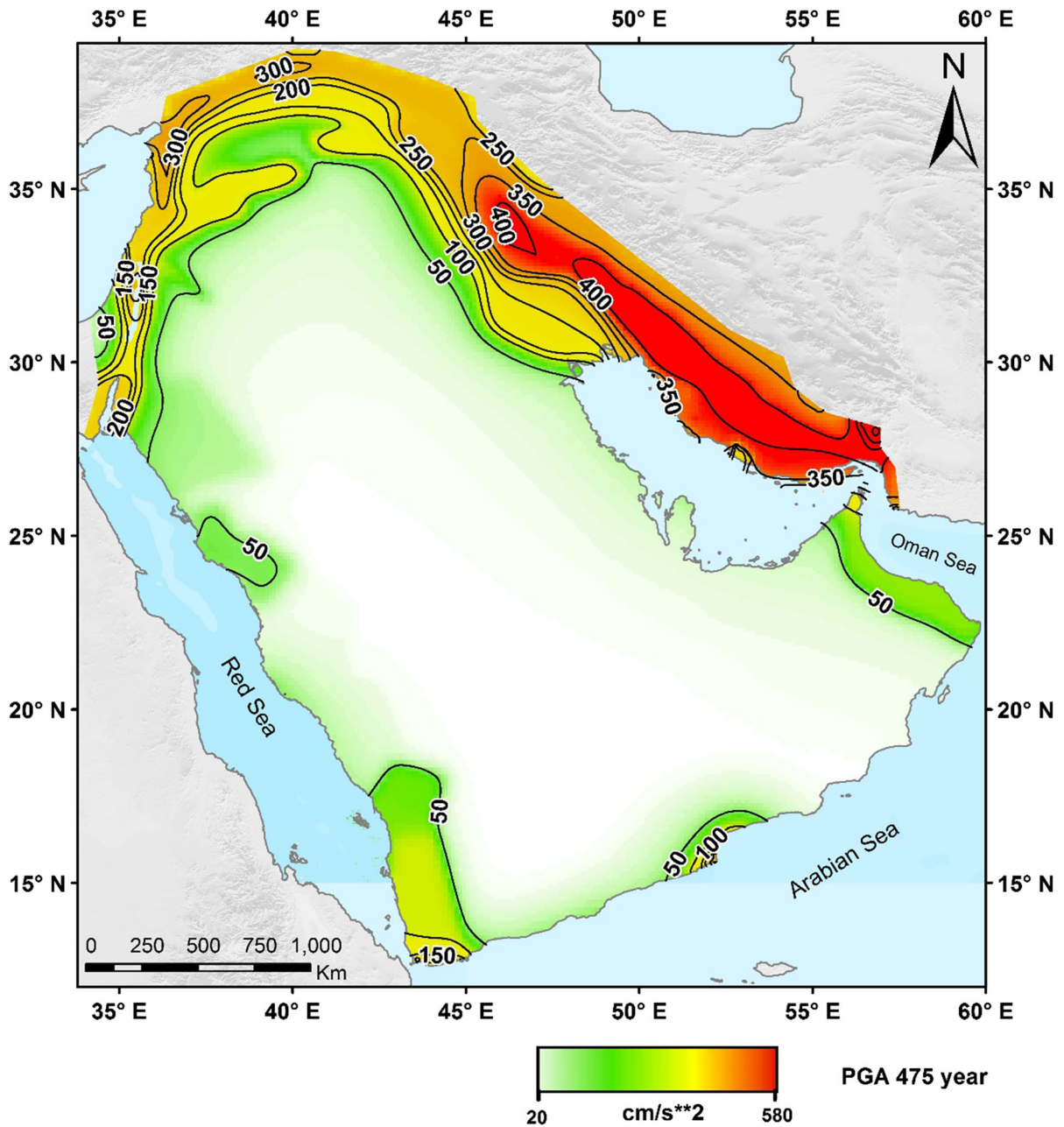


Figure 6

Probabilistic seismic hazard in terms of PGA in cm/s^2 at bedrock conditions for return period of 475 years in the Arabian Plate

Reduction Program (NEHRP) site classification ($V_{S30} \geq 760$ m/s, where V_{S30} is the average shear-wave velocity in the uppermost 30 m of the site). All the maps are available on the website of the Earthquake Monitoring Center (EMC) of Sultan Qaboos University (SQU) (<https://www.squ.edu.om/emc/>

[hazardmaps](#)). Herein, maps of PGA and horizontal SA for 0.2 s (short period) and 1 s at return periods of 475 and 2475 years are presented. These maps with the selected spectral periods will facilitate development of design response spectra analogous to European or American styles of seismic code.

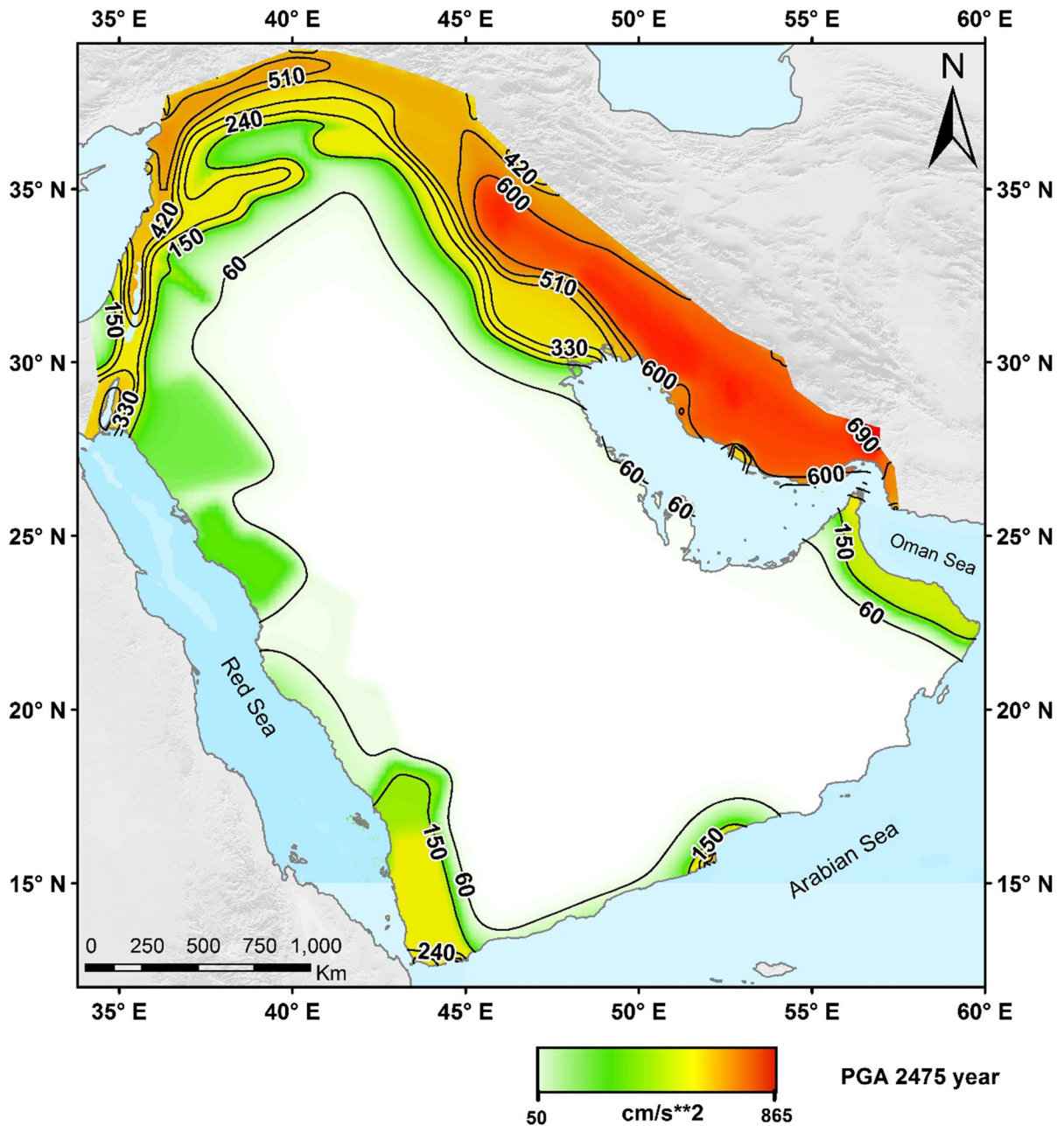


Figure 7

Probabilistic seismic hazard in terms of PGA in cm/s^2 at bedrock conditions for return period of 2475 years in the Arabian Plate

The PGA across the Arabian Peninsula and its surroundings ranged between about 20 cm/s^2 and about 580 cm/s^2 for the return period of 475 years, and between 50 and 865 cm/s^2 for the return period of 2475 years (Figs. 6, 7). The Zagros zone, which shows high seismic hazard values, is located

geographically outside the Arabian Peninsula to the northeast, so it is not considered in the discussion below. The most hazardous regions in the Arabian Peninsula are located along the Gulf of Aqaba–Dead Sea Fault, with PGA of about 270 cm/s^2 for the return period of 475 years at the northern and middle parts

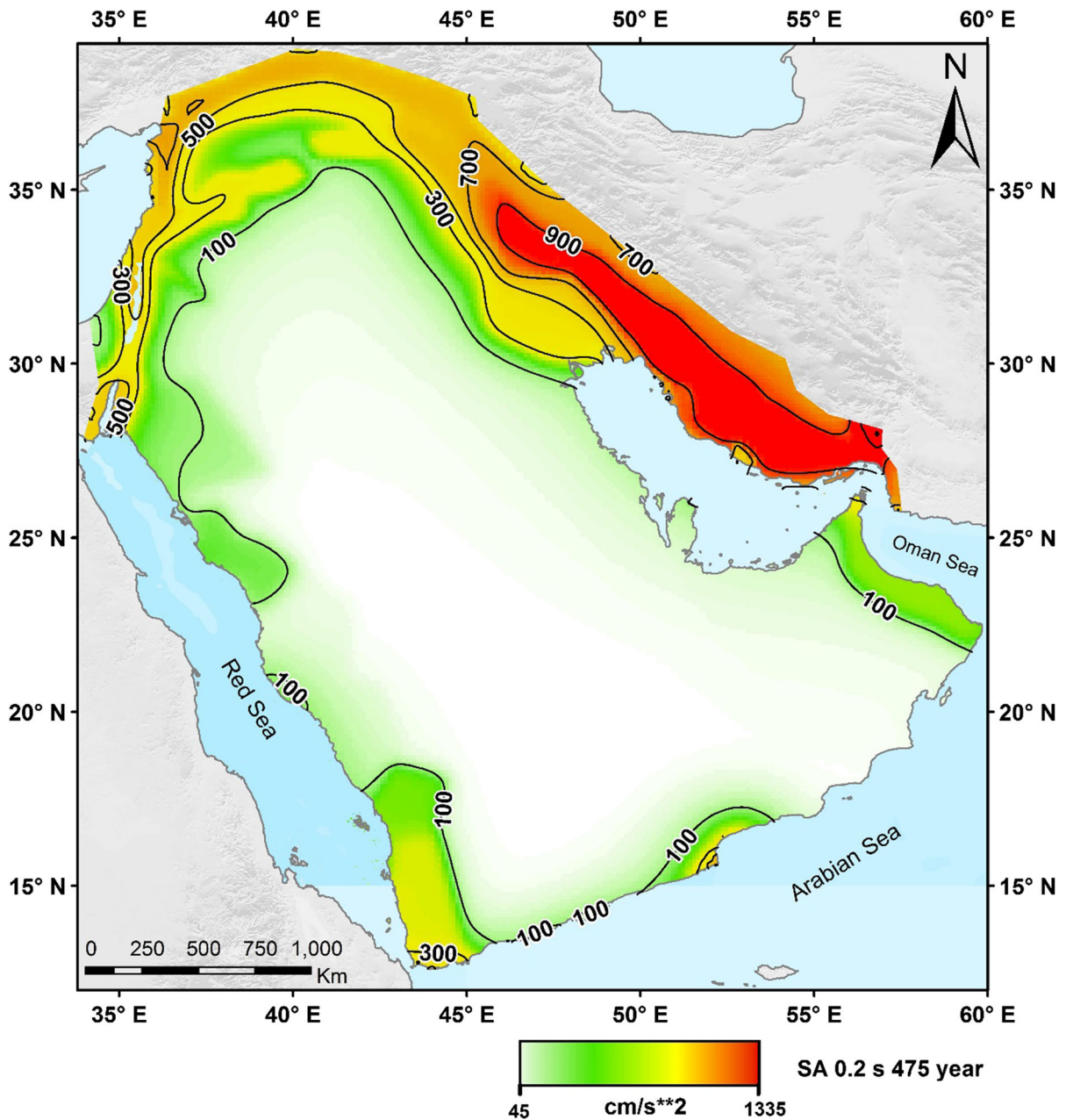


Figure 8

Probabilistic seismic hazard in terms of spectral acceleration (SA) at spectral period of 0.2 s in cm/s^2 at bedrock conditions for the return period of 475 years in the Arabian Plate

of the fault. Areas of relatively high seismic hazard are distributed in Yemen, along the Iraq–Iran border, Northern Syria, and the northernmost parts of Oman (Figs. 6, 7). With the exception of these relatively high hazard areas, the maps reveal that the majority

of the Arabian Peninsula is characterized by relatively low seismic hazard, as the PGA values do not exceed 50 cm/s^2 for the return period of 475 years. This delineates the interior of the Arabian Peninsula from the relatively threatened regions along the major

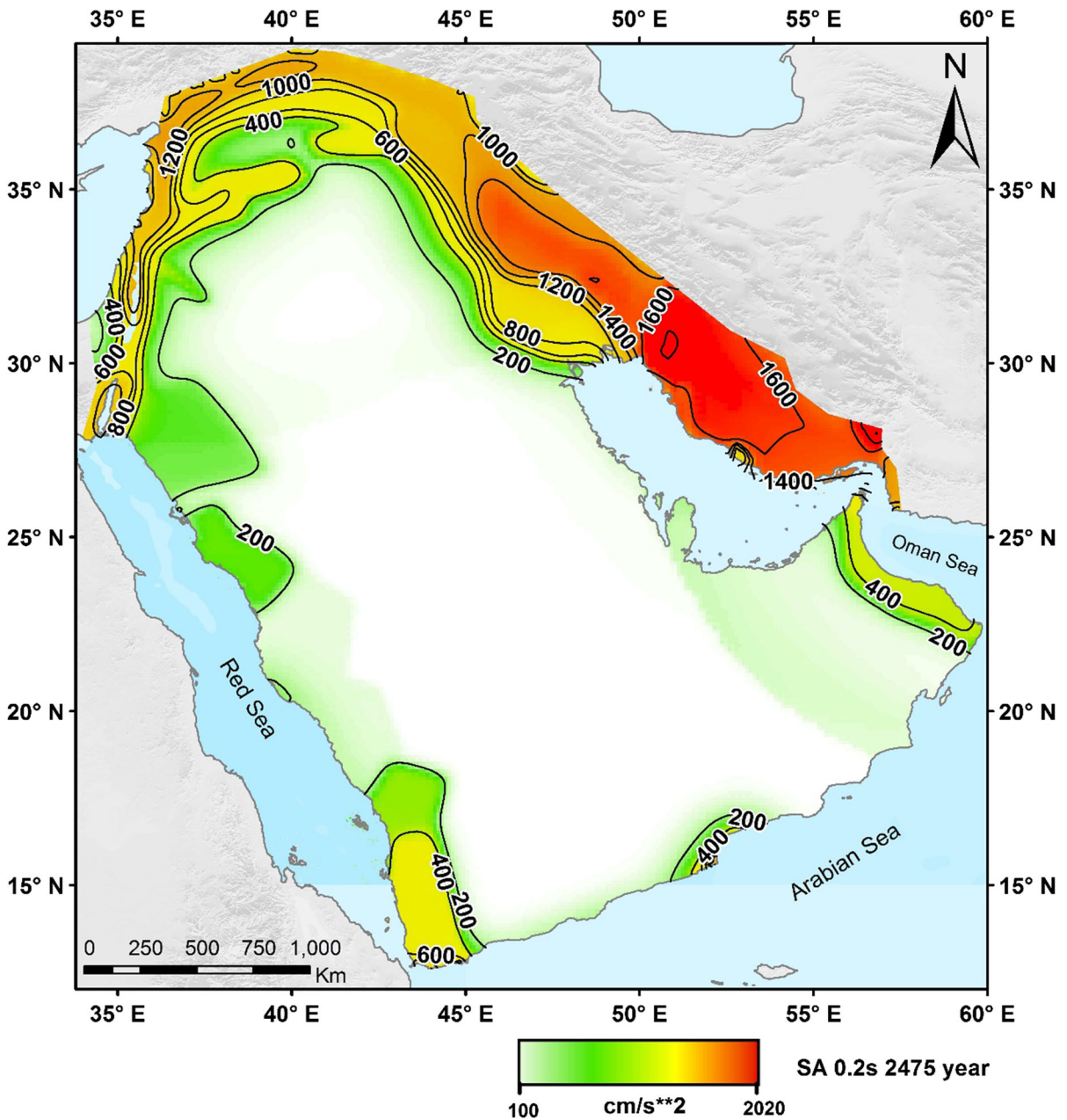


Figure 9

Probabilistic seismic hazard in terms of SA at spectral period of 0.2 s in cm/s^2 at bedrock conditions for the return period of 2475 years in the Arabian Plate

active structures at the border areas of the Arabian Plate.

The pattern of the seismic hazard maps is strongly associated with the geometry of the implemented seismic source models, and the shapes of the hazard maps do not change significantly when changing the

mapped spectral period. Thus, the seismic hazard maps reflect the typical seismotectonic setting of the Arabian Peninsula.

Figures 8 and 9 show the 5% damped horizontal spectral acceleration at spectral period of 0.2 s for the return periods of 475 and 2475 years. The maximum

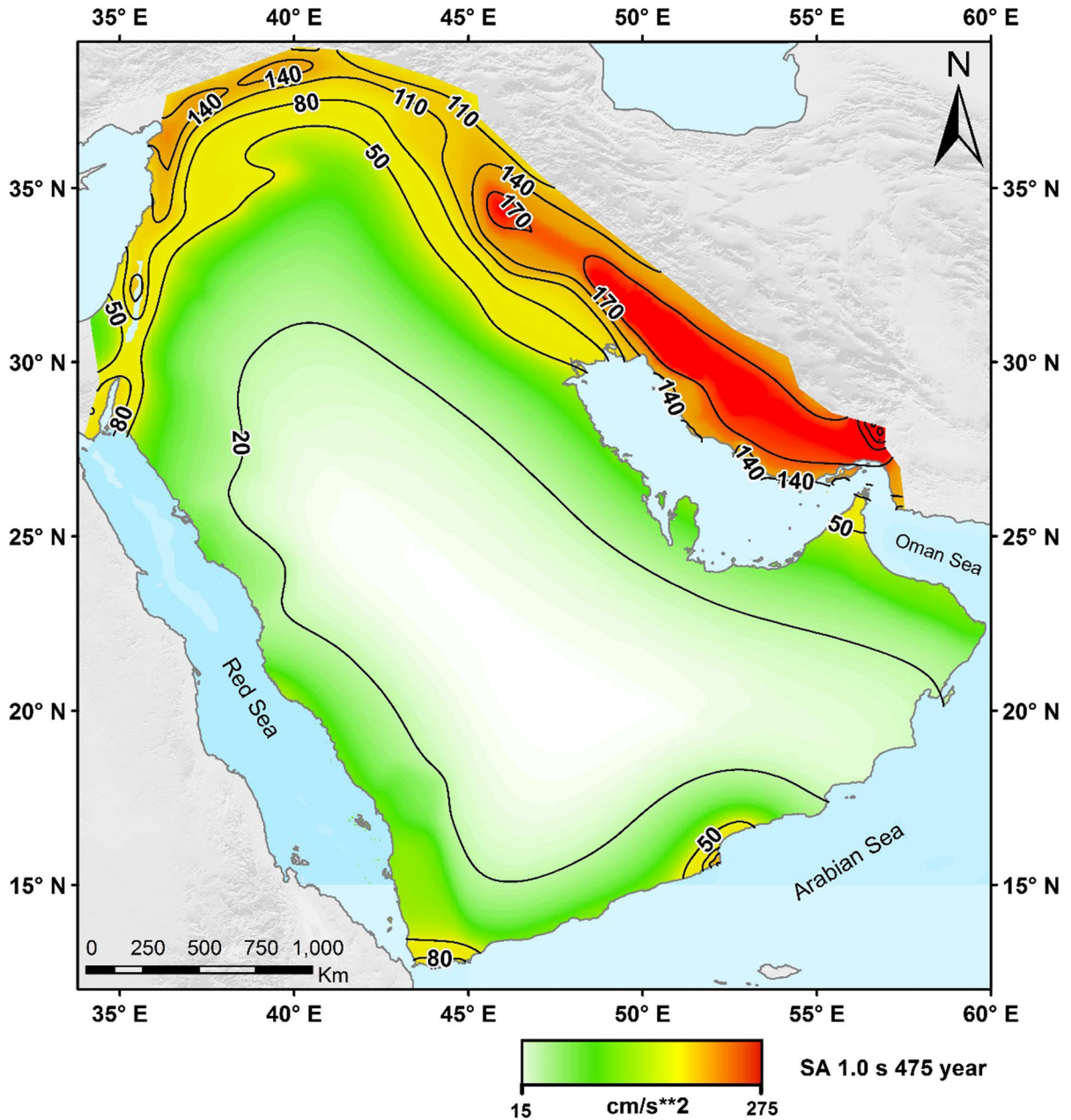


Figure 10

Probabilistic seismic hazard in terms of SA at spectral period of 1.0 s in cm/s^2 at bedrock conditions for the return period of 475 years in the Arabian Plate

ground-motion values are found to be associated with the spectral period of 0.2 s for the entire area of study, with maximum ground motion of about 630 cm/s^2 at the Gulf of Aqaba–Dead Sea Fault for the return period of 475 years. This spectral period is

very important, as it is the natural period of two-storey buildings, which are very common in many countries on the Arabian Peninsula.

The hazard values for the spectral period of 1 s (Figs. 10, 11) are lower than those for shorter periods

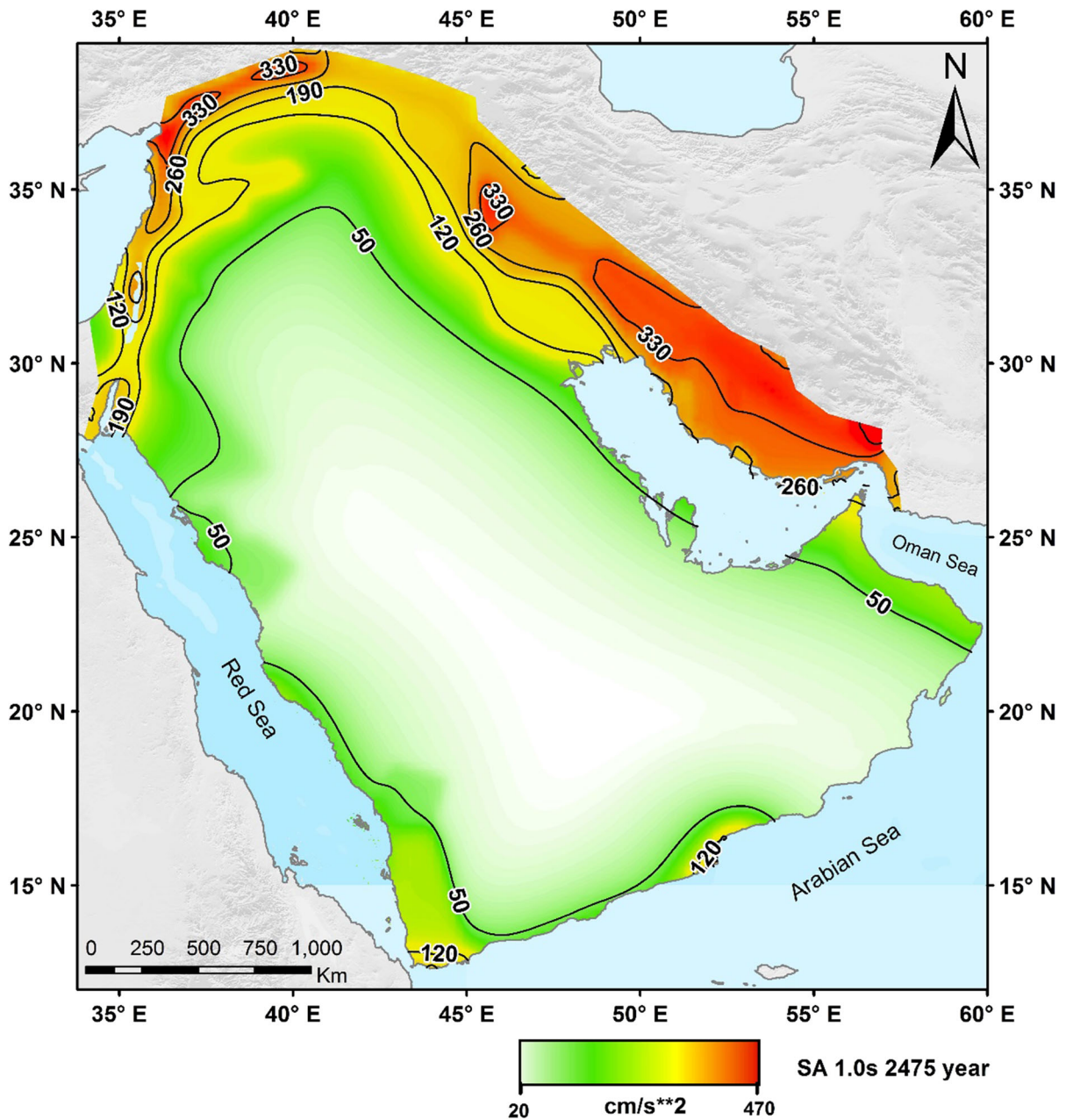


Figure 11

Probabilistic seismic hazard in terms of SA at spectral period of 1.0 s in cm/s^2 at bedrock conditions for the return period of 2475 years in the Arabian Plate

(0.1 and 0.2 s). Moreover, note that the high hazard in these maps exhibits a less steep gradient than on the 0.2 s maps, indicating faster attenuation of short-period ground motion with distance. The consequence is that adjacent sites may have different short-period hazards.

The PGA levels for the return period of 2475 years are 70% to about 100% higher than those for the return period of 475 years for most of the sites studied. Similar relationships are reported in literature (Peláez et al. 2006; Hamdache et al. 2012; Sawires et al. 2016). Figure 12a, b depicts highly

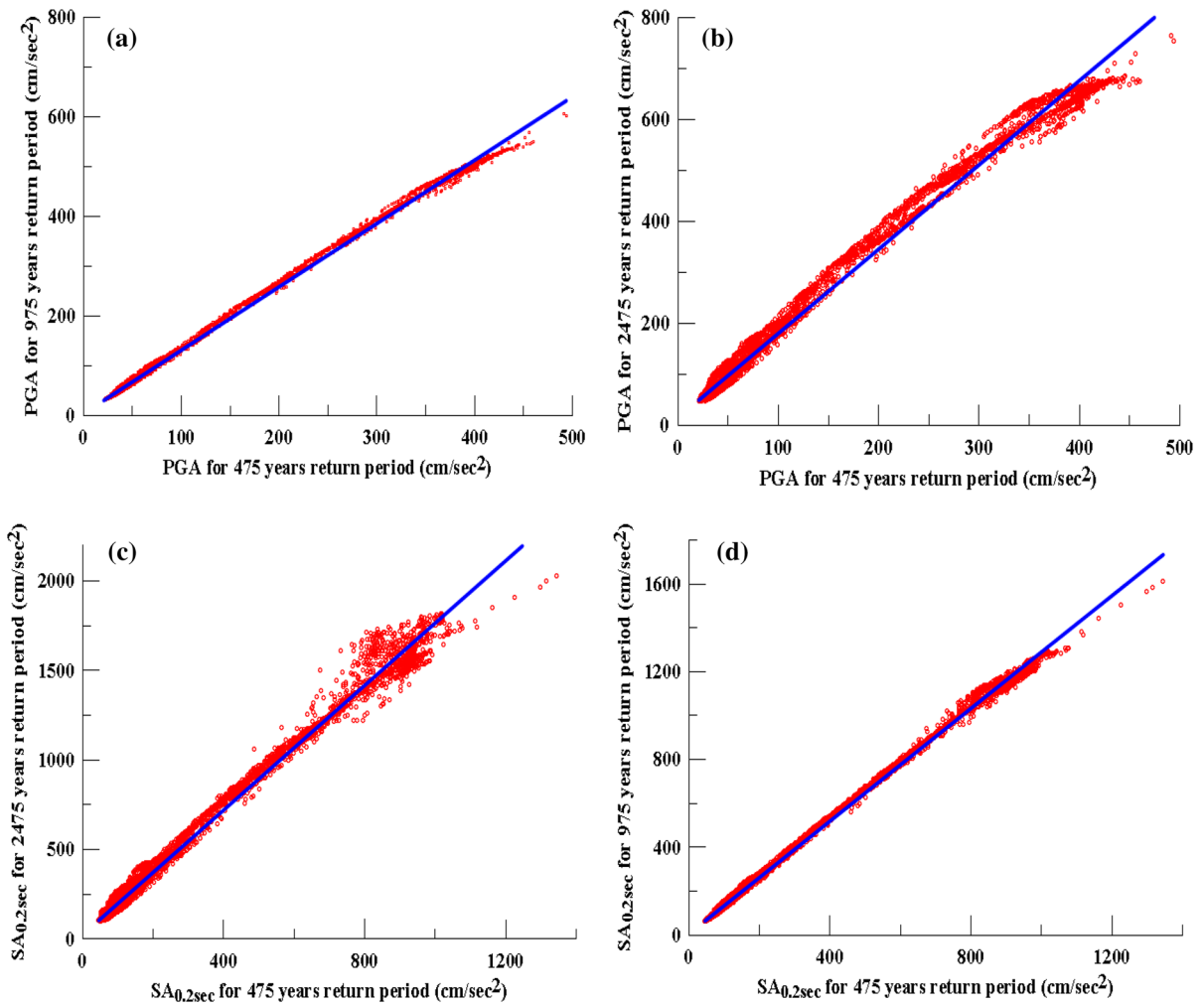


Figure 12

High-correlation relationships between PGA (a, b) and SA for 0.2 s (c, d) hazard values at the return period of 475 years and those at return periods of 975 and 2475 years

consistent relationships between the PGA (cm/s²) at the return period of 475 years versus PGA (cm/s²) at the return periods of 975 and 2475 years:

$$PGA_{975} (cm/s^2) = 1.27PGA_{475} (cm/s^2) + 4.13 (R^2 = 0.9985), \quad (6)$$

$$PGA_{2475} (cm/s^2) = 1.75PGA_{475} (cm/s^2) + 15.73 (R^2 = 0.9931). \quad (7)$$

Almost similar relations were found for the SA at 0.2 s (Fig. 12c, d), indicating the possibility of computing an approximate ground motion for a specific spectral period and return period in the

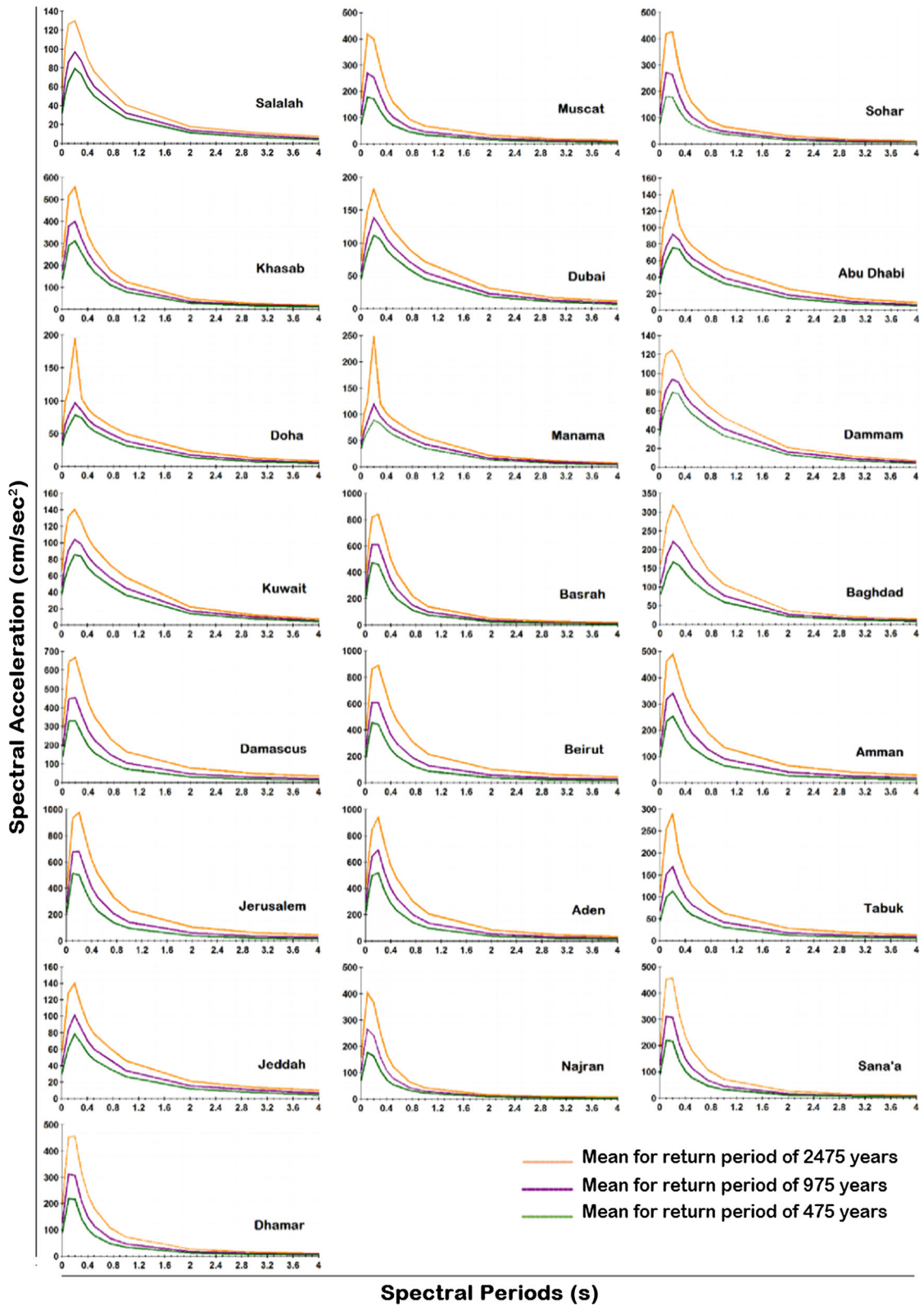
Arabian Peninsula if the ground motion at the same spectral period is known for another return period.

$$SA_{0.2,975} (cm/s^2) = 1.28SA_{0.2,475} (cm/s^2) + 5.51 (R^2 = 0.9986), \quad (8)$$

$$SA_{0.2,2475} (cm/s^2) = 1.74SA_{0.2,475} (cm/s^2) + 25.31 (R^2 = 0.9928). \quad (9)$$

Figure 13

Average horizontal component unified hazard spectrum (UHS) at 5% damping for return periods of 475, 975 and 2475 years



In the current PSHA, the uniform hazard spectrum (UHS) at 22 significant population centers was obtained by calculating the probabilistic seismic hazard (PSH) at a group of spectral periods by applying the aforementioned GMPEs. Therefore, the ground motion was computed separately for each considered spectral period. The ground motion of each spectral period was then identified for a specific return period (e.g., 475 years) and plotted against the corresponding spectral period, yielding the UHS. These UHS show the variation and the period dependence of the seismic hazard across the Arabian Peninsula at Salalah, Muscat, Sohar, Khasab, Dubai, Abu Dhabi, Doha, Manama, Dammam, Kuwait, Basra, Baghdad, Damascus, Beirut, Amman, Jerusalem, Aden, Tabuk, Jeddah, Najran, Sana'a, and Dhamar (Fig. 13). PGA and spectral accelerations at some important engineering spectral periods are presented in Table 4.

5. Discussion

The hazard maps presented herein show the PSH to be reasonable using existing data and information, considering the limited scientific knowledge and detailed studies regarding the seismogenic nature of many areas in the region. Instrumentally recorded earthquakes indicate that most of the Arabian Plate appears to be aseismic. However, historical records of strong shaking at Qalhat, Nizwa, Sohar, Najran, Taief, Makah, Al-Madinah, and Tabuk are warnings that a probable significant seismic hazard may occur within the Arabian Plate. Therefore, further studies on active faulting and paleoseismicity, including geological field investigations of the reported shaking in such areas, could serve to confirm or deny the historical reports. The consequence is that the hazard can be tied to specific faults rather than an average over broad areas, resulting in a more accurate and more localized seismic hazard.

The results of the present SHA are based on the postulation that the future locations of large earthquakes will lie within the identified seismic zones, which could be false as some seismic zones (e.g., the Gulf of Aqaba and the Makran Subduction Zone) have shown seismic quiescence for considerably

longer periods of time, while this may not be the case in the future. This confirms the critical need for studying the active faulting in the area of interest.

As the GMPEs play a crucial role in the SHA, it might be important to install integrated strong-motion networks for continuous recording throughout the countries on the Arabian Plate to provide essential data required for developing specific GMPEs based upon actual data collected from various surrounding tectonic environments. Linking these strong-motion networks, and exchanging their data and results, would ultimately result in a wider magnitude and distance spectra and thus a better GMPE for SHA.

Like recent PSH analysis, uncertainties associated with input parameters were incorporated into the hazard analysis to account for epistemic variations. The PGA hazard results for the return period of 475 years in the present study have been compared with those of Al-Haddad et al. (1994). The seismic hazard values of the current study are higher than those calculated by Al-Haddad et al. (1994) for the eastern area of the Arabian Peninsula, where they mapped 475-year seismic hazard levels below 50 cm/s^2 . The PGA values of Al-Haddad et al. (1994) are higher in the southwestern part of Saudi Arabia with ground-motion above 250 cm/s^2 . The shape and hazard values of the PGA hazard maps of the two studies differ for the following reasons: (1) the current study used an updated catalogue and more recent GMPEs tested in the Middle East, (2) the current study considered the Oman Mountains and southeastern Turkey as seismic sources, (3) different seismic source models were adopted in the two studies, and (4) uncertainties in the input parameters are treated appropriately herein. One similarity between the two studies is the high hazard estimates for the Gulf of Aqaba–Dead Sea Fault, even though the seismic source model used by Al-Haddad et al. (1994) did not contain as many specific sources as provided herein. Generally, the hazard values of the current study are inconsistent with those calculated by the EMME project (Danciu et al. 2017) for the well-constrained common areas of the two studies. The present work, therefore, may represent the seismic hazard in the Arabian Plate better than the three previous hazard studies (Al-Haddad et al. 1992, 1994; Pascucci et al. 2008).

Table 4
PGA and spectral accelerations at some important engineering spectral periods

City	Coordinates		PGA (cm/s ²)			0.2 s (cm/s ²)			0.5 s (cm/s ²)			1.0 s (cm/s ²)			2.0 s (cm/s ²)		
	Lat.	Long.	475	975	2475	475	975	2475	475	975	2475	475	975	2475	475	975	2475
Salahat	17.05	54.11	35.92	45.62	62.16	87.83	108.63	143.99	55.46	67.50	85.13	28.97	35.26	45.22	12.58	15.52	20.08
Muscat	23.59	58.41	79.11	115.43	178.22	181.70	264.30	414.25	77.73	110.56	172.43	38.68	52.09	77.06	17.80	25.09	38.98
Sohar	24.35	56.71	78.68	114.20	175.45	184.06	266.98	422.88	80.38	109.98	166.95	41.00	52.71	73.38	17.65	23.64	34.93
Khasab	26.16	56.24	146.53	189.02	252.83	337.69	432.89	592.42	179.49	225.39	296.79	82.85	103.34	133.79	30.29	38.32	51.77
Dubai	25.20	55.27	45.98	56.97	75.20	111.08	136.94	181.17	79.29	95.65	121.00	45.61	56.55	73.43	18.72	23.92	32.91
Abu Dhabi	24.45	54.38	32.22	40.15	54.23	75.32	92.21	136.46	52.65	62.28	77.57	32.08	39.19	50.73	14.51	18.70	26.58
Doha	25.29	51.53	32.21	40.05	54.17	76.53	94.43	157.05	52.23	61.80	77.08	30.89	37.59	48.46	13.63	17.38	24.13
Manama	26.23	50.59	35.88	44.31	60.19	86.89	110.57	185.15	59.87	71.50	89.96	34.57	42.44	55.00	13.92	17.26	22.59
Dammam	26.42	50.09	33.23	41.24	55.98	77.72	93.33	125.67	54.56	64.74	81.19	32.03	39.10	50.56	13.08	16.21	21.31
Kuwait	29.31	47.48	38.06	48.16	67.37	88.04	109.13	151.10	61.43	74.39	95.26	35.58	43.94	57.11	13.75	16.98	22.00
Basra	30.51	47.78	192.95	257.00	354.39	437.42	580.79	806.41	181.58	246.21	355.86	71.10	93.42	130.34	24.59	32.20	45.61
Baghdad	33.31	44.36	88.76	119.98	174.61	189.92	251.86	363.37	122.58	161.32	227.86	61.58	80.33	111.26	22.25	28.55	39.33
Damascus	33.51	36.28	174.18	238.62	347.69	407.16	552.53	807.01	189.63	273.77	430.62	84.36	123.54	200.19	36.14	55.62	95.19
Beirut	33.89	35.50	211.42	287.86	413.21	486.84	660.23	954.31	217.44	316.97	501.83	94.18	139.71	230.53	39.74	61.83	107.33
Amman	31.95	35.93	91.24	121.54	173.05	217.63	290.42	414.18	119.07	164.42	241.47	58.81	82.55	121.46	25.44	37.08	58.57
Jerusalem	31.77	35.21	208.12	284.07	407.25	484.71	658.61	951.54	224.94	327.60	507.15	96.61	144.11	234.65	40.06	63.89	108.19
Tabuk	28.38	36.57	45.20	67.33	109.25	109.65	162.64	272.66	56.61	79.52	123.13	29.31	40.40	60.72	12.53	17.71	27.32
Jeddah	21.49	39.19	34.03	45.42	65.15	86.07	112.39	157.20	52.16	66.79	88.63	29.02	37.28	50.86	13.08	17.13	23.06
Najran	17.57	44.23	61.49	92.32	144.78	141.74	211.02	333.34	51.32	73.14	115.09	23.05	30.03	42.31	8.97	11.73	16.03
Sana'a	15.37	44.19	92.88	130.01	196.00	221.10	310.02	463.34	80.59	118.08	188.35	34.06	47.64	75.21	13.32	18.51	28.76
Aden	12.79	45.02	210.42	277.82	376.89	500.43	657.37	892.62	224.61	310.59	450.44	96.73	132.70	198.12	38.54	54.57	82.27
Dhahran	14.55	44.41	93.24	130.36	196.34	221.98	310.97	464.22	81.47	118.89	189.20	35.72	48.77	75.96	13.96	19.04	29.23

No comparison was made with the PGA map for the return period of 475 years of the Seismic Hazard Assessment Program (GSHAP), as the hazard values in the GSHAP for major parts of the Arabian Peninsula are not the outcome of real hazard estimation. The hazard assessment in these areas was extrapolated from the hazard in surrounding regions (the Gulf of Aqaba–Dead Sea Fault and Zagros Belt) without accounting for local seismicity, in order not to leave gaps in a worldwide map (Grunthal et al. 1999). The authors are not aware of any maps of SA covering the entire Arabian Peninsula for comparison with the results of the current study. The hazard maps provided in the current study will permit engineers to create approximate UHS for their particular sites in bedrock conditions for the Arabian Peninsula, reflecting the expected ground shaking at several important spectral periods.

The provided PSH maps describe the ground motion at flat bedrock conditions, not taking into account amplification of ground motion due to the presence of soft soils or topographic features. These site conditions could, particularly, amplify long-period ground motion generated by large earthquakes around the Arabian Peninsula, affecting real-estate wealth. Therefore, coupling the current results with site-specific characteristics is best practice to fully obtain seismic design coefficients for sites with ground conditions that differ from flat rock, especially for critical and important facilities.

Moreover, ground failure hazards (e.g., surface rupture, liquefaction, and landslide) were not considered in the current analysis. Full understanding of seismic hazards will require identification of areas susceptible to these secondary ground failure hazards.

6. Conclusions

This study presents a new, justifiable PSHA for the Arabian Peninsula in terms of PGA and 5% damped spectral accelerations at bedrock conditions for return periods of 475, 975, and 2475 years. The current PSH maps were created based on existing data, adapting the recent state of knowledge; they could be updated as more data become available. The analyses were conducted within a logic-tree framework, considering uncertainties in the source model,

recurrence parameters, maximum earthquake, and GMPE. The results show that low hazard levels with expected horizontal PGA less than 50 cm/s^2 for the return period of 475 year dominate the majority of the Arabian Peninsula. The contour maps illustrated herein will allow engineers to construct a UHS for each particular site in the Arabian Peninsula, reflecting the ground shaking at spectral periods of interest.

The results of the present study may contribute substantially to developing a unified GCC Seismic Building Code, an ambitious project that is currently underway. Additionally, these results could provide relevant seismic hazard parameters for planners, regulators, and engineers to minimize earthquake effects, allow design of earthquake-resistant structures, and determine whether retrofitting is required for existing structures in the Arabian Peninsula.

REFERENCES

- Akkar, S., & Bommer, J. J. (2010). Empirical equations for the prediction of PGA, PGV and spectral accelerations in Europe, the Mediterranean region and the Middle East. *Seismological Research Letters*, 81, 195–206.
- Aldama, B. (2009). *An exploratory study of parameter sensitivity, representation of results and extension of PSHA: case study- United Arab Emirates*. PhD thesis, Imperial College London.
- Aldama, B., Bommer, J. J., Fenton, C. H., & Stafford, P. J. (2009). Probabilistic seismic hazard analysis for rock sites in the cities of Abu Dhabi, Dubai and Ra's Al Khaymah, United Arab Emirates. *Georisk*, 3, 1–29.
- Al-Haddad, M., Siddiqi, G. H., Al-Zaid, R., Arafah, A., Necioglu, A., & Turkelli, N. (1992). Seismic hazard and design criteria for Saudi Arabia. In *Earthquake engineering, tenth world conference, Balkem, Rotterdam*, ISBN:9054100605.
- Al-Haddad, M., Siddiqi, G. H., Al-Zaid, R., Arafah, A., Necioglu, A., & Turkelli, N. (1994). A basis for evaluation of seismic hazard and design criteria for Saudi Arabia. *Earthquake Spectra*, 10, 231–258.
- Allen, M., Jackson, J. A., & Walker, R. (2004). Late Cenozoic reorganization of the Arabia-Eurasia collision and the comparison of short-term and long-term deformation rates. *Tectonics*, 23, TC2008.
- Ambraseys, N. N., & Jackson, J. A. (1998). Faulting associated with historical and recent earthquakes in the Eastern Mediterranean region. *Geophysical Journal International*, 133, 390–406.
- Ambraseys, N. N., & Melville, C. P. (1982). *A history of Persian earthquakes*. Cambridge: Cambridge University Press.
- ArRajehi, A., McClusky, S., Reilinger, R., Daoud, M., Alchalbi, A., Ergintav, S., et al. (2010). Geodetic constraints on present-day motion of the Arabian Plate: Implications for Red Sea and Gulf of Aden rifting. *Tectonics*, 29, TC3011.

- ASC. (2003). 1945—Off the Makran Coast (Balochistan), Pakistan, M_w 8.0. Amateur Seismic Center, <http://asc-india.org/gq/mekran.htm>.
- Atkinson, G. M., & Boore, D. M. (2003). Empirical ground-motion relations for subduction-zone earthquakes and their application to Cascadia and other regions. *Bulletin of Seismological Society of America*, 93, 1703–1729.
- Atkinson, G. M., & Boore, D. M. (2006). Earthquake ground-motion prediction equations for Eastern North America. *Bulletin of Seismological Society of America*, 96, 2181–2205.
- Babiker, N., Mula, A., & El-Hadidy, S. (2015). A unified M_w -based earthquake catalogue and seismic source zones for the Red Sea. *Journal of African Earth Sciences*, 109, 168–176.
- Bartov, Y., Steinitz, G., Eyal, M., & Eyal, Y. (1980). Sinistral movement along the Gulf of Aqaba—its age and relation to the opening of the Red Sea. *Nature*, 285, 220–222.
- Bayrak, Y., Öztürk, A. S., Çınara, H., Kalafat, D., Tsapanos, T. M., Koravos, G. Ch., et al. (2009). Estimating earthquake hazard parameters from instrumental data for different regions in and around Turkey. *Engineering Geology*, 105, 200–210.
- Bender, B. K., & Perkins, D. M. (1982). *SEISRISK III: A computer program for seismic hazard estimation*. U.S. Geological Survey Open File Report 82–293.
- Berberian, M. (1995). Master ‘blind’ thrust faults hidden under the Zagros folds, active basement tectonics and surface morphotectonics. *Tectonophysics*, 241, 193–224.
- Beyer, K., & Bommer, J. J. (2006). Relationships between median values and between aleatory variabilities for different definitions of the horizontal component of motion. *Bulletin of Seismological Society of America*, 96, 1512–1522. (Erratum (2007) 97, 1769)
- Bommer, J. J., Scherbaum, F., Bungum, H., Cotton, F., Sabetta, F., & Abrahamson, N. A. (2005). On the use of logic-trees for ground-motion prediction equations in seismic hazard analysis. *Bulletin of Seismological Society of America*, 95, 377–389.
- Bulut, F., Marco, B., Tuna, E., Janssen, C., Kılıç, T., & Dresen, G. (2012). The East Anatolian Fault Zone: Seismotectonic setting and spatiotemporal characteristics of seismicity based on precise earthquake locations. *Journal of Geophysical Research*, 117, B07304.
- Burkhard, M., & Grunthal, G. (2009). Seismic source zone characterization for the seismic hazard assessment project PEGASOS by the Expert Group 2 (EG 1b). *Swiss Journal of Geosciences*, 102, 149–188.
- Campbell, K. (2003). Prediction of strong ground-motion using the hybrid empirical method and its use in the development of ground-motion (attenuation) relations in Eastern North America. *Bulletin of Seismological Society of America*, 93, 1012–1033.
- Chiou, B. S., & Youngs, R. R. (2008). An NGA model for the average horizontal component of peak ground motion and response spectra. *Earthquake Spectra*, 24, 173–215.
- Coleman, R. G. (1993). *Geologic evolution of the Red Sea*. Oxford monographs on geology and geophysics (Vol. 24). Oxford: Oxford University Press.
- Cornell, C. A. (1968). Engineering seismic risk analysis. *Bulletin of Seismological Society of America*, 18, 1583–1606.
- Cornell, C. A., & Vanmarcke, E. H. (1969). The major influences on seismic risk. In *Proceedings of the fourth world conference of earthquake engineering*, 1, Santiago, Chile, 69–83.
- Cosentino, P., Ficarra, V., & Luzio, D. (1977). Truncated exponential frequency-magnitude relationship in earthquake statistics. *Bulletin of the Seismological Society of America*, 67, 1615–1623.
- Cramer, H. (1961). *Mathematical methods of statistics* (2nd ed.). Princeton: Princeton University Press.
- Danciu, L., Sesetyan, K., Demircioglu, M., Gulen, L., Zare, M., Basili, R., et al. (2017). The 2014 earthquake model of the middle east: seismogenic sources. *Bulletin of Earthquake Engineering*, 22, 22. <https://doi.org/10.1007/s10518-017-0096-8>.
- Deif, A., Abou-Elenean, K., El-Hadidy, M., Tealeb, A., & Mohamed, A. (2009). Probabilistic seismic hazard maps for Sinai Peninsula, Egypt. *Journal of Geophysics and Engineering*, 6, 288–297.
- Deif, A., Al-Shijbi, Y., El-Hussain, I., Ezzelarab, M., & Mohamed, A. M. E. (2017). Compiling an earthquake catalogue for the Arabian Plate, Western Asia. *Journal of Asian Earth Sciences*, 147, 345–375.
- Deif, A., & El-Hussain, I. (2012). Seismic moment rate and earthquake mean recurrence interval in the major tectonic boundaries around Oman. *Journal of Geophysics and Engineering*, 9, 773–783.
- Delavaud, E., Cotton, F., Akkar, S., Scherbaum, F., Danciu, L., Beauval, C., et al. (2012). Towards a ground-motion logic-tree for probabilistic seismic hazard assessment in Europe. *Journal of Seismology*, 16, 451–473.
- DeMets, C. (2008). *Arabia’s slow dance with India*, Nature Geoscience 1, 10–11, der Schweiz. Ph.D. thesis, ETH-Zurich.
- Dong, W. M., Bao, A. B., & Shah, H. C. (1984). Use of maximum entropy principle in earthquake recurrence relationships. *Bulletin of the Seismological Society of America*, 74, 725–737.
- Douglas, J., Akkar, S., Ameri, G., Bard, P. Y., Bindi, D., Bommer, J., et al. (2014). Comparisons among the five ground-motion models developed using RESORCE for the prediction of response spectral accelerations due to earthquakes in Europe and the Middle East. *Bulletin of Earthquake Engineering, Springer Verlag*, 12, 341–358.
- El-Hussain, I., Al-Shijbi, Y., Deif, A., Mohamed, A. M. E., & Ezzelarab, M. (2018). Developing a seismic source model for the Arabian Plate. *Arabian Journal of Geosciences*, 11, 435. <https://doi.org/10.1007/s12517-018-3797-7>.
- El-Hussain, I., Deif, A., Al-Jabri, K., Toksoz, N., El-Hady, S., Al-Hashmi, S., et al. (2012). Probabilistic seismic hazard maps for Sultanate of Oman. *Natural Hazards*, 64, 173–210.
- Erdik, M., Demircioglu, B., Sesetyan, K., & Durukal, E. (2008). *Probabilistic seismic hazard assessment for Dubai*. Boğaziçi University, Kandilli Observatory and Earthquake Research Institute, Department of Earthquake Engineering, unpublished report.
- Farhoudi, G., & Karig, D. E. (1977). Makran of Iran and Pakistan as an active arc system. *Geology*, 5, 664–668.
- Fenton, C. H., Adams, J., & Halchuk, S. (2006). Seismic hazard assessment for radioactive waste disposal sites in regions of low seismic activity. *Geotechnical and Geological Engineering*, 24, 579–592.
- Fournier, M., Chamot-Rooke, N., Petit, C., Fabbri, O., Huchon, P., Maillot, B., et al. (2008). In-situ evidence for dextral active motion at the Arabia-India plate boundary. *Nature Geoscience, Nature Publishing Group*, 1, 54–58.
- Gardner, J. K., & Knopoff, L. (1974). Is the sequence of earthquakes in Southern California, with aftershocks removed, Poissonian? *Bulletin of Seismological Society of America*, 64, 1363–1367.
- Girdler, R. W., & Underwood, M. (1985). The evolution of early oceanic lithosphere in the southern Red Sea. *Tectonophysics*, 116, 95–108.

- Grunthal, G., Bosse, C., Sellami, S., Mayer-Rosa, D., & Giardini, D. (1999). Compilation of the GSHAP regional seismic hazard map for Europe, Africa and the Middle East. *Annali di Geofisica*, 42, 1215–1223.
- Grunthal, G., & Wahlstrom, R. (2012). The European-Mediterranean Earthquake Catalogue (EMEC) for the last millennium. *Journal of Seismology*, 16, 535–570.
- Gutenberg, B., & Richter, C. F. (1956). Magnitude and energy of earthquakes. *Annali di Geofisica*, 9, 1–15.
- Haghipour, A., Chorashi, M., & Kadjar, M. (1984). *Explanatory text of the seismotectonic map of Iran, Afghanistan and Pakistan, Commission for geological map of world-UNESCO*. Tehran: Geological Survey of Iran.
- Hamdache, M., Peláez, A. J., Talbi, A., Mobarki, M., & López Casado, C. L. (2012). Ground-motion hazard values for Northern Algeria. *Pure and Applied Geophysics*, 169, 711–723. <https://doi.org/10.1007/s00024-011-0333-z>.
- Hessami, K., Jamali, F., & Tabassi, H. (2003). *Major active faults in Iran*. Ministry of Science, Research and Technology, International Institute of Earthquake Engineering and Seismology (IIEES), 1:250000 scale map.
- Huijjer, C., Harajli, M., & Sadek, S. (2016). Re-evaluation and updating of the seismic hazard of Lebanon. *Journal of Seismology*, 20, 233–250.
- Johnson, P. R. (1998). *Tectonic map of Saudi Arabia and adjacent areas*. Deputy Ministry for Mineral Resources, USGS TR-98-3, Saudi Arabia.
- Kijko, A. (2004). Estimation of the maximum earthquake magnitude M_{max} . *Pure and Applied Geophysics*, 161, 1655–1681.
- Kijko, A., & Sellevoll, M. A. (1992). Estimation of earthquake hazard parameters from incomplete data files Part II: Incorporation of magnitude heterogeneity. *Bulletin of the Seismological Society of America*, 82(1), 120–134.
- Kijko, A., & Singh, M. (2011). Statistical tools for maximum possible earthquake magnitude estimation. *Acta Geophysica*, 59(4), 674–700. <https://doi.org/10.2478/s11600-011-0012-6>.
- Lloyd's City Risk Index (2015). *Middle East cities* [online]. https://www.lloyds.com/cityriskindex/locations/region/middle_east.
- McGuire, R. K. (1978). *FRISK: Computer program for seismic risk analysis using faults as earthquake sources*. U.S. Geological Survey Open-File Report 78-1007.
- Musson, R. M. W. (2009). Subduction in the Western Makran: the historian's contribution. *Journal of Geological Society, London*, 166, 387–391.
- Onur, T., Gok, R., Abdalnaby, W., Shakir, A., Mahdi, H., Numan, N., Al-Shukri, H., Chalib, H., Ameen, T., & Abd, N. (2016). Probabilistic seismic hazard assessment for Iraq. Lawrence Livermore National Laboratory, LLNL-TR-691152.
- Palano, M., Paola Imprescia, P., & Gresta, S. (2013). Current stress and strain-rate fields across the Dead Sea fault system: constraints from seismological data and GPS observations. *Earth Planetary Science Letters*, 369–370, 305–316.
- Pararas-Carayannis, G. (2004). Seismo-dynamics of compressional tectonic collision-potential for tsunami genesis along boundaries of the Indian, Eurasian and Arabian plates. In *Abstract submitted to the International Conference HAZARDS*, Hyderabad, India, 2–4 Dec. 2004.
- Pascucci, V., Free, M. W., & Lubkowski, Z. A. (2008). Seismic hazard and seismic design requirements for the Arabian Peninsula. (Online). In *The 14th world conference on earthquake engineering*, October 12–17, 2008, Beijing, China.
- Peláez, A. J., Hamdache, M., & López Casado, C. L. (2006). Seismic hazard in terms of spectral accelerations and uniform hazard spectra in Northern Algeria. *Pure and Applied Geophysics*, 163, 119–135. <https://doi.org/10.1007/s00024-005-0011-0>.
- Rasul, N. M. A., Stewart, I. C. F., & Nawab, Z. A. (2015). Introduction to the Red Sea: Its origin, structure, and environment. In N. M. A. Rasul & C. F. Stewart (Eds.), *The Red Sea* (pp. 1–28). Berlin, Heidelberg: Springer.
- Salamon, A., Avraham, H., Garfunkel, Z., & Ron, H. (2003). Seismotectonics of Sinai subplate-Eastern Mediterranean region. *Geophysical Journal International*, 155, 149–173.
- Sawires, R., Peláez, J. A., Fat-Helbary, R. E., & Ibrahim, H. A. (2016). Updated probabilistic seismic hazard values for Egypt. *Bulletin of the Seismological Society of America*, 106(4), 1788–1801. <https://doi.org/10.1785/0120150218>.
- Sneh, A. (1996). The Dead Sea Rift: Lateral displacement and down faulting phases. *Tectonophysics*, 263, 277–292.
- Stoneley, R. (1974). Evolution of the continental margins bounding a former Tethys. In C. A. Burk & C. L. Drake (Eds.), *The geology of continental margins* (pp. 889–903). New York: Springer.
- Tavakoli, B., & Ghafari-Ashtiany, M. (1999). Seismic hazard assessment of Iran. *Annali di Geofisica*, 42, 1013–1021.
- Uhrhammer, R. (1986). Characteristics of northern and southern California seismicity. *Earthquake Notes*, 113, 57–61.
- Vermeulen, P., & Kijko, A. (2017). More statistical tools for maximum possible earthquake magnitude estimation. *Acta Geophysica*. <https://doi.org/10.1007/s11600-017-0048-3>.
- Vernant, P. H., Nilforoushan, F., Hatzfeld, D., Abassi, M. R., Vigny, C., Masson, F., et al. (2004). Present-day crustal deformation and plate kinematics in Middle East constrained by GPS measurements in Iran and northern Oman. *Geophysical Journal International*, 157, 381–398.
- Weichert, D. H. (1980). Estimation of the earthquake recurrence parameters for unequal observation periods for different magnitudes. *Bulletin of Seismological Society of America*, 70, 1337–1346.
- Yilmaz, N., & Yucemen, S. M. (2015). Sensitivity of seismic hazard results to alternative seismic source and magnitude-recurrence models: a case study for Jordan. *Geodinamica Acta*, 27, 189–202.
- Youngs, R. R., Chiou, S. J., Silva, W. J., & Humphrey, J. R. (1997). Strong ground motion attenuation relationships for subduction zone earthquakes. *Seismological Research Letters*, 68, 58–73.
- Zahran, H. M., Sokolov, V., Roobol, J., Stewart, I. C. F., El-Hadidy, S. Y., & El-Hadidy, M. (2016). On the development of a seismic source zonation model for seismic hazard assessment in western Saudi Arabia. *Journal of Seismology*, 20, 747–769.
- Zhao, J. X., Zhang, J., Asano, A., Ohno, Y., Oouchi, T., Takahashi, T., et al. (2006). Attenuation relations of strong ground motion in Japan using site classification based on predominant period. *Bulletin of the Seismological Society of America*, 96, 898–913.